Downloaded from rspa.royalsocietypublishing.org on February 28, 2013

PROCEEDINGS OF THE ROYAL SOCIETY A MATHEMATICAL, PHYSICAL & ENGINEERING SCIENCES

The Morphology and Mechanism of Formation of Porous Anodic Films on Aluminium

J. P. O'Sullivan and G. C. Wood

Proc. R. Soc. Lond. A 1970 **317**, doi: 10.1098/rspa.1970.0129, published 7 July 1970

References

Article cited in:
http://rspa.royalsocietypublishing.org/content/317/1531/511#related-urls

Email alerting service

Receive free email alerts when new articles cite this article - sign up in the box at the top right-hand corner of the article or click **here**

To subscribe to *Proc. R. Soc. Lond. A* go to:
http://rspa.royalsocietypublishing.org/subscriptions

Downloaded from rspa.royalsocietypublishing.org on February 28, 2013

Proc. Roy. Soc. Lond. A. **317**, 511–543 (1970)
Printed in Great Britain

The morphology and mechanism of formation of porous anodic films on aluminium

By J. P. O'Sullivan† and G. C. Wood

Corrosion Science Division, Department of Chemical Engineering, University of Manchester Institute of Science and Technology, P.O. Box 88, *Sackville Street, Manchester M* 60 1*QD*

(*Communicated by Sir Nevill Mott, F.R.S.—Received* 24 *November* 1969)

[Plates 7 to 12]

The morphology of porous anodic oxide films formed on aluminium in phosphoric acid electrolytes at constant current density or voltage, and under changing electrical or electrolytic conditions, has been studied quantitatively by electron microscopy. Replicas from film sections and from both film interfaces have been prepared, as well as transmission micrographs of thin films, produced under accurately defined conditions.

During formation at constant current density, pore initiation occurs by the merging of locally thickening oxide regions, which seem related to the substructure of the substrate, and the consequent concentration of current into the residual thin areas. The pores grow in diameter and change in number until the steady-state morphology is established.

The film barrier layer thickness has been measured directly for the first time. The steady-state barrier-layer thickness, cell diameter and pore diameter are all observed to be directly proportional to the formation voltage. It becomes evident that the barrier-layer thickness, decided largely by an equilibrium established between oxide formation in the barrier-layer and field-assisted dissolution (probably thermally enhanced) at the pore bases, determines the cell and pore sizes by a simple geometrical mechanism. Anion incorporation into the film and its hydrogen-bonded structure play secondary roles to these factors in determining the actual film morphology, although not its subsequent properties. A consequence of the mechanism is that, at constant current density, relatively non-aggressive electrolytes give thicker barrier layers, larger cells and larger pores next to the barrier layer than aggressive media, although subsequent pore widening at the outer surface of the film by simple chemical dissolution is more severe in aggressive electrolytes.

1. Introduction

Porous anodic films, formed on aluminium by anodizing in acid electrolytes, have attracted considerable research because of their importance in the surface finishing of aluminium and because their mechanism of formation represents an almost unique situation in the field of anodic processes. The present paper presents new, directly measured, data on the morphology of these films and suggests mechanisms explaining the findings.

Following earlier optical and electron optical observations, electron micrographs in the now classical paper of Keller, Hunter & Robinson (1953) were interpreted as showing a thick outer layer, containing fine, regular, almost cylindrical, parallel-sided pores, perpendicular to the macroscopic surface of the specimen, penetrating a close-packed hexagonal, cellular structure and extending from the outer surface as far as a thin, compact, scalloped, barrier layer which separated the porous layer

† See note on p. 542.

The Royal Society is collaborating with JSTOR to digitize, preserve, and extend access to *Proceedings of the Royal Society of London. Series A, Mathematical and Physical Sciences.* www.jstor.org

Downloaded from rspa.royalsocietypublishing.org on February 28, 2013

from the metal. The diameter of the oxide cells was approximately twice the barrier-layer thickness and proportional to the forming voltage, each cell containing a single star-shaped pore, whose dimensions were supposedly independent of voltage but dependent upon the electrolyte type and conditions. It was postulated (Keller *et al.* 1953; Hunter & Fowle 1954*b*) that the structure maintained itself during growth by the development of regions of hot, concentrated acid at the pore bases, which permitted the local rate of dissolution to keep up with the over-all growth rate. The remarkable regularity of the pores was first demonstrated in section by Booker, Wood & Walsh (1957) and various minor changes in morphology have been noted by other investigators (Renshaw 1961; Zalivalov, Tyukina & Tomashov 1961; Franklin & Stirland 1963; Paolini, Masoeri, Sacchi & Paganelli 1965).

Certain refinements and criticisms of this model have been suggested subsequently. Thus, Hoar & Mott (1959) indicated that it was unnecessary to postulate the hot, concentrated acid at the pore bases, the high dissolution rates there being explicable in terms of field-assisted dissolution. Murphy & Michelson (1962) actually considered the pores to be of secondary importance and emphasized the significance of more randomly arranged, hydrogen-bonded regions, containing the acid anion, which separated fine sub-microcrystallites of largely anhydrous oxide, in determining the film structure and conduction through it. They suggested, without direct visual evidence, that growth occurred in a transition region between the barrier layer and the porous layer. These last concepts have received some incomplete support from the infrared spectroscopy studies of Dorsey (1968, 1969) and from the observation of 'fibrous' structures by Ginsberg & Wefers (1963), the fibres being hollow cylinders of alumina containing water and the acid anion, and the fibre bundles of Csokan (1964).

Regarding the pore initiation stages rather than the above steady-state situation, Hoar & Yahalom (1963) suggested that, during constant voltage anodizing, local, field-retarded proton action on the barrier layer explained the approximately close-packed, hexagonal array of pores more satisfactorily than specific acid attack of pre-existing cell centres, richer in more soluble amorphous alumina than the outer regions, as inferred by Franklin (1957).

The recent finding by Wood, O'Sullivan & Vaszko (1968) that, by using electrolyte conditions which would sustain a high film formation voltage, films with barrier layers and pore structures readily observable *in detail* by replica and transmission electron microscopy could be produced, prompted the present study. Certain new facts emerge which permit the proposal of relatively simple mechanisms explaining most of the known features of these films.

2. Experimental procedure

Spade electrodes, usually $20 \times 10 \times 1$ mm, of 99.99 % aluminium (Cu 0.002, Fe 0.004, Si 0.003 wt %), or occasionally zone-refined aluminium (Ca 10, Cu 10, Mn 20, Mg 20 parts/10^6 by wt), were electropolished individually in a perchloric acid/ethanol

Downloaded from rspa.royalsocietypublishing.org on February 28, 2013

bath, washed and dried. Anodic films were then formed on the individual specimens in vigorously stirred electrolyte within ± 0.5 K of the set temperature, under the conditions described in the various sections, washed in distilled water and ethanol and dried in a cold air stream. Cell voltage–time curves at constant current density or current–time curves at constant voltage were obtained on a fast recorder. In certain experiments, the potential of the anodizing electrode was measured by using a calomel electrode, via a probe and an agar bridge, so that the contributions of the potential drop between the electrodes and the cathodic overpotential to the cell voltage could be estimated. The value was only about 0.5 V, so could be neglected.

Anodizing was performed in 0.4, 1.5 or 2.5 M† phosphoric acid, with occasional runs in 0.2 M oxalic acid, 1.5 M sulphuric acid or 0.17 M ammonium tartrate solution with its pH adjusted to 7. All solutions were prepared from Analar reagents and doubly distilled water condensed on Pyrex. Film thicknesses were controlled by anodizing under conditions predetermined to give the correct values, using metallography of sections or assessment of the electrical curves for thick and thin films respectively. Anodizing was usually carried out at as high a current density and voltage as possible in relatively dilute acid at a low temperature, thus promoting large cell, pore and barrier layer dimensions. Perusal of the data of Spooner & Seraphim (1954) suggested that the optimum conditions for this purpose would be to use various times at 80 to 120 V or 50 to 100 A m^{-2} in 0.4 M phosphoric acid at 25 °C and these were the most commonly employed.

The anodized specimen was bent into a V-shape, producing cracks in the oxide parallel to the specimen sides which had not been bent. After removing excess debris with distilled water in an ultrasonic cleaner and drying, direct carbon replicas of the film surfaces and exposed cleavage planes were prepared by depositing a thin layer of carbon onto the specimen. These were shadowed with Pt/C mixture, deposited at an angle of incidence of 60°, but in the same vertical plane as the direction of the cracks in order to give maximum contrast. The replicas were stripped by immersion in 0.25 M hydrofluoric acid (made up with a 50:50 mixture of water and ethanol), which dissolved the oxide film, permitting the replica fragments to float free. The collected replicas were then dipped in 3 M hydrochloric acid to remove excess oxide before a final wash in distilled water. The replicas, which tended to dry in a flattened form, apparently revealing film surfaces and sections in the same plane (O'Sullivan 1968; Wood & O'Sullivan 1969), were examined in an AEI E.M. 6 electron microscope.

Replicas on film surfaces alone were scored into small squares before immersion in the HF solution. In order to examine the underside of the oxide, it was replicated similarly after removal from the aluminium using 0.2 M mercuric chloride solution. Replication of the metal surface beneath a film was performed after the film above had been dissolved in a solution of 35 ml phosphoric acid (85 %) and 0.02 kg of chromic acid made up to 1 l with water. For transmission electron microscopy of thin films, the films were removed after scoring by amalgamation of the substrate

† M signifies mole/litre.

Downloaded from rspa.royalsocietypublishing.org on February 28, 2013

and examined immediately after washing and drying in cold air. Further details are given elsewhere (O'Sullivan 1968).

Measurements of film dimensions were made directly on the photographic plates, using a travelling microscope. Periodic calibration of the magnification of the electron microscope revealed a likely maximum error of 3 to 5 %.

3. Results and interpretation

(a) *General film morphology*

Figure 1, plate 7, illustrates many general features of the steady-state films, as revealed by replica electron microscopy. Thus, figure 1*a* shows the film detached from the metal in the region of the barrier layer, the barrier layer itself, the pores and cell structure and the way in which the semi-spherical faces of the oxide cells protruded into the metal being clearly evident. The pores are less ideally revealed by the fracture in figure 1*b* but here the metal substrate was still attached to the

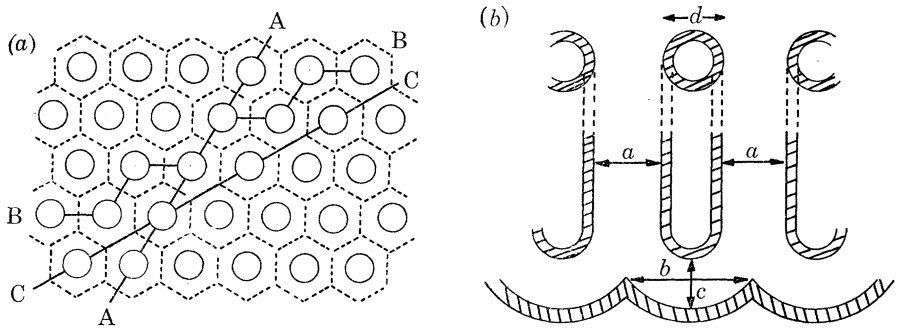

Figure 2. (*a*) Possible cleavage planes obtained upon fracturing a porous anodic film (after Booker *et al.* (1967)). (*b*) Schematic diagram of carbon replicas taken from film surfaces and fracture sections (shaded areas represent regions where the oxide replica is thick). $a = 2 \times$ cell-wall thickness; b = cell diameter; c = barrier-layer thickness; d = pore diameter.

film. Examination of many sections confirmed that fractures did not occur regularly over the whole oxide surface revealed. For example, figure 1*a* shows that pores on different planes were displayed, pores often appearing not to extend through the film thickness merely because the fracture face changed direction. Furthermore, apparent pore diameters varied considerably (figure 1*b*), so attempts were not generally made to measure pore dimensions from film sections, except in certain cases where large changes in pore diameter would be expected and a general trend readily detectable.

Figure 2*a* is a schematic diagram, (after Booker *et al.* 1957), illustrating the possible cleavage planes produced upon fracture. Clearly the apparent pore diameter varies with the cleavage plane. If the fracture occurs through AA or CC the pore diameters would appear to be similar, providing fracture is through the pore centres,

Downloaded from rspa.royalsocietypublishing.org on February 28, 2013

(*a*)

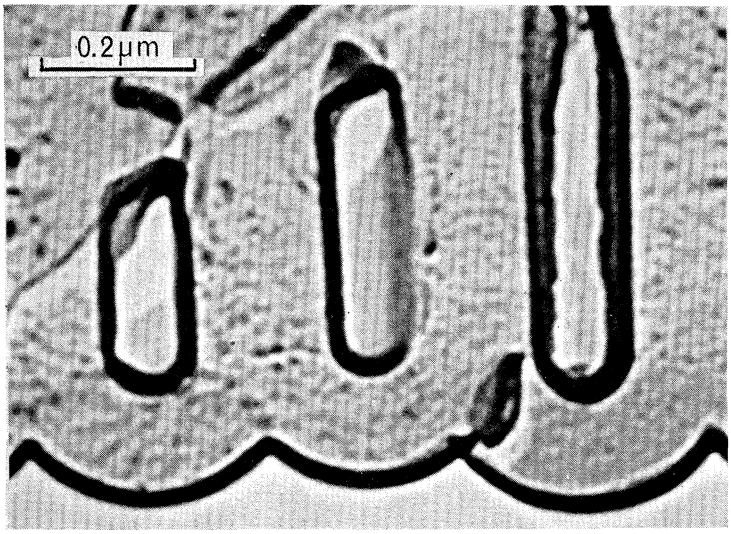

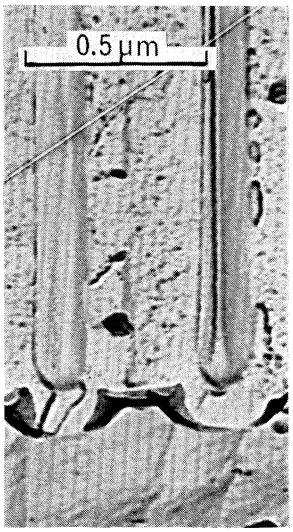

(*b*)

(*c*)

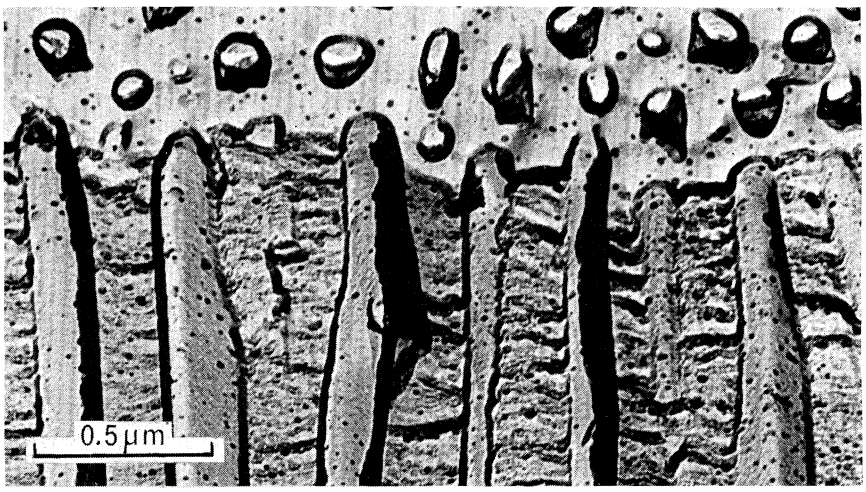

(*d*)

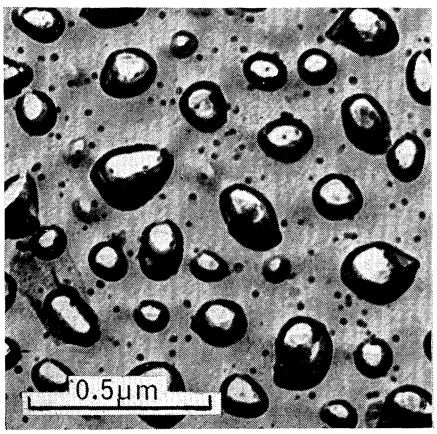

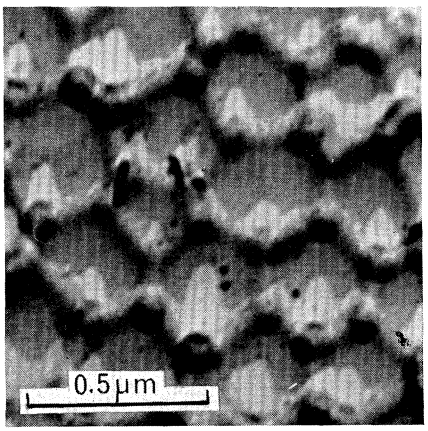

(*e*)

FIGURE 1. Replica electron micrographs of anodic films formed in phosphoric acid, showing general film characteristics: (*a*) section near barrier layer; (*b*) section with metal attached to the film base; (*c*) section near outer surface; (*d*) film outer surface; (*e*) metal surface after removal of the film. The films were formed at 120 V for (*a*) and (*b*), 145 V for (*c*) and (*d*) and 100 V for (*e*).

(*Facing p.* 514)

Downloaded from rspa.royalsocietypublishing.org on February 28, 2013

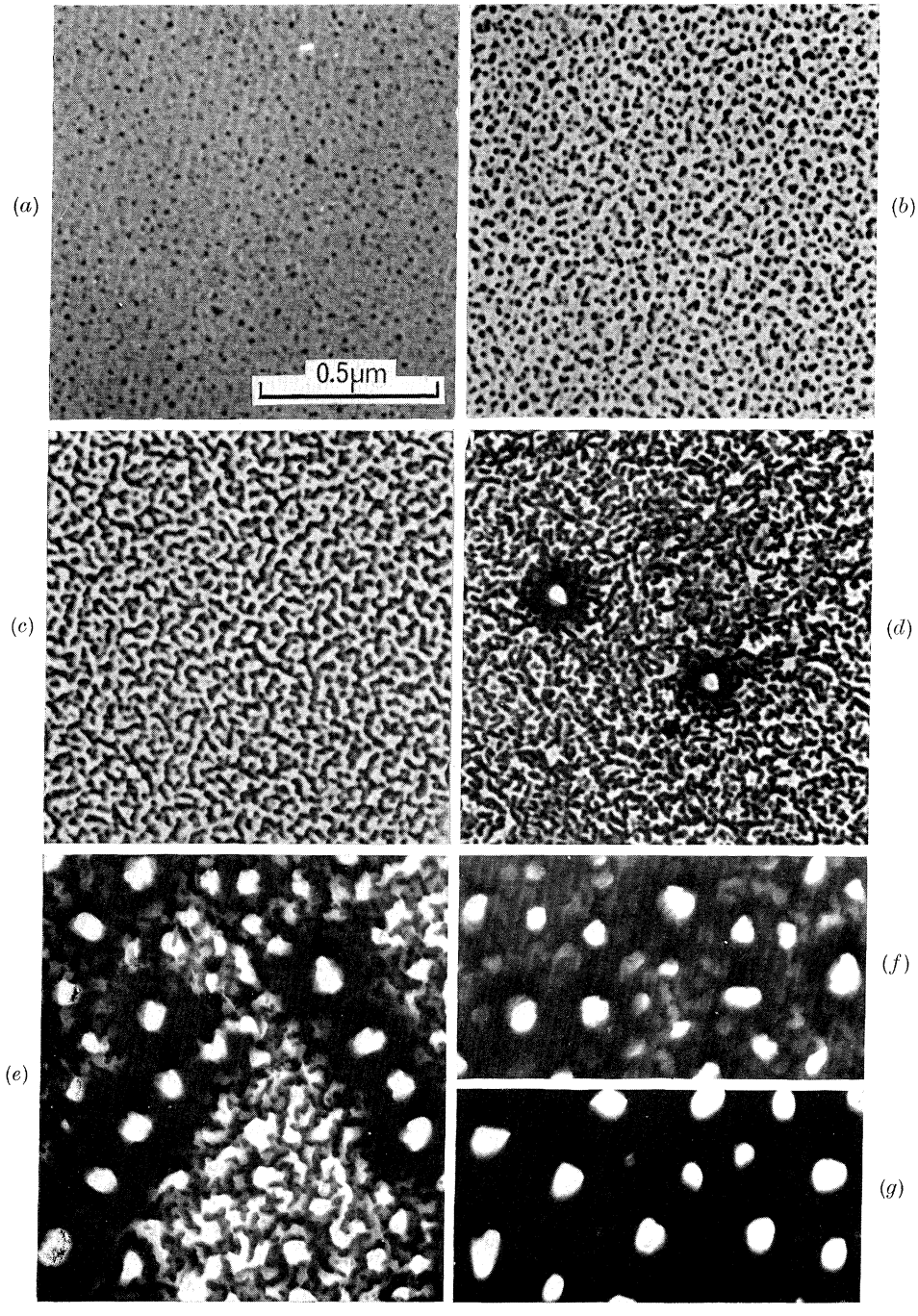

FIGURE 5. Transmission electron micrographs of films grown at 50 A m^{-2} in 0.4 M phosphoric acid at 25 °C for (*a*) 40 s, (*b*) 80 s, (*c*) 120 s, (*d*) 160 s, (*e*) 200 s, (*f*) 280 s and (*g*) 330 s, showing 'nuclei', incipient pores and major pore development.

Downloaded from rspa.royalsocietypublishing.org on February 28, 2013

(*a*)

(*b*)

(*c*)

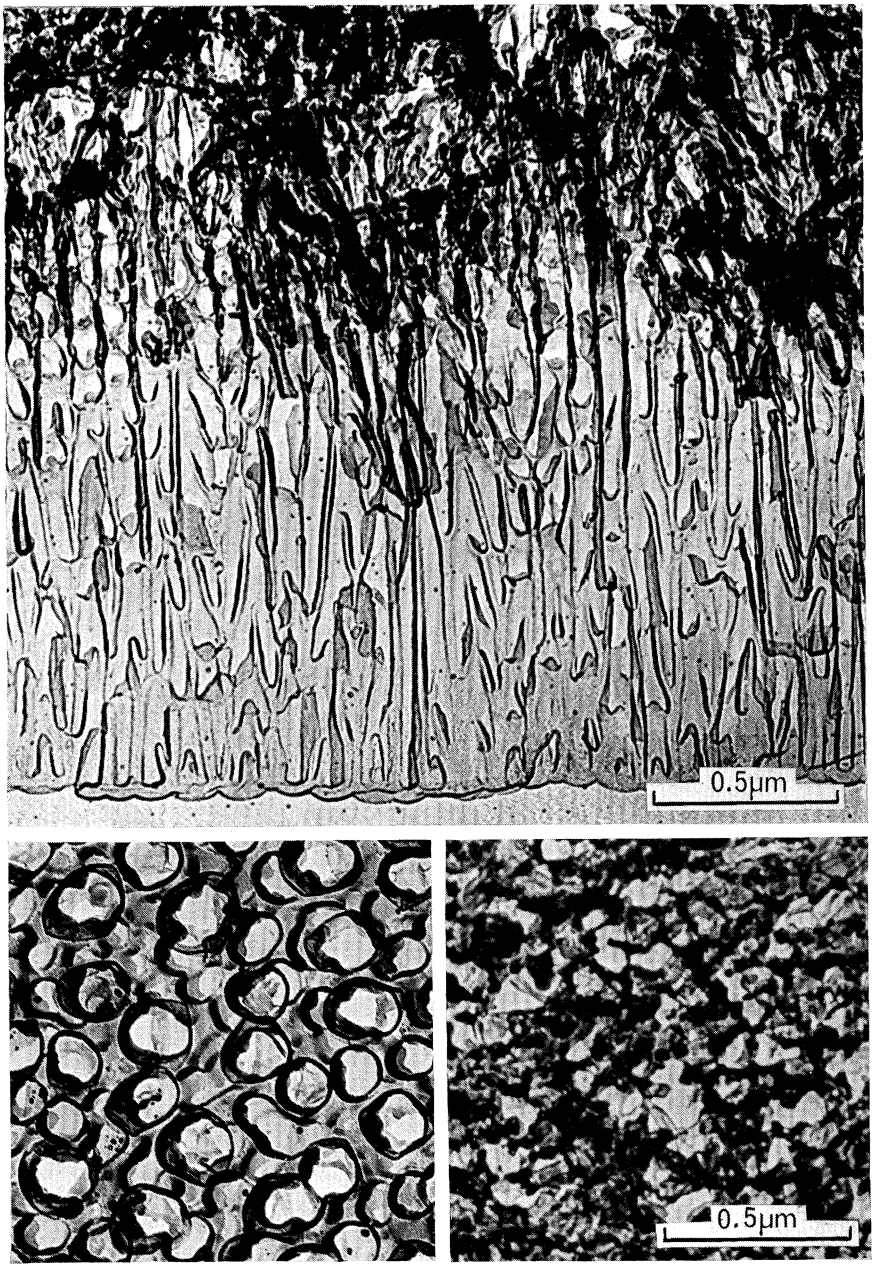

FIGURE 10. Electron micrographs, showing attack of outer regions of films by aggressive electrolytes: (*a*) section of 30 V film formed in 2.5 M phosphoric acid at 25 °C; (*b*) surface of film formed at 100 A m^{-2} in 0.4 M phosphoric acid at 30 °C; and (*c*) surface of film formed at 100 A m^{-2} in 2.5 M phosphoric acid at 25 °C.

Downloaded from rspa.royalsocietypublishing.org on February 28, 2013

(*a*)

(*b*)

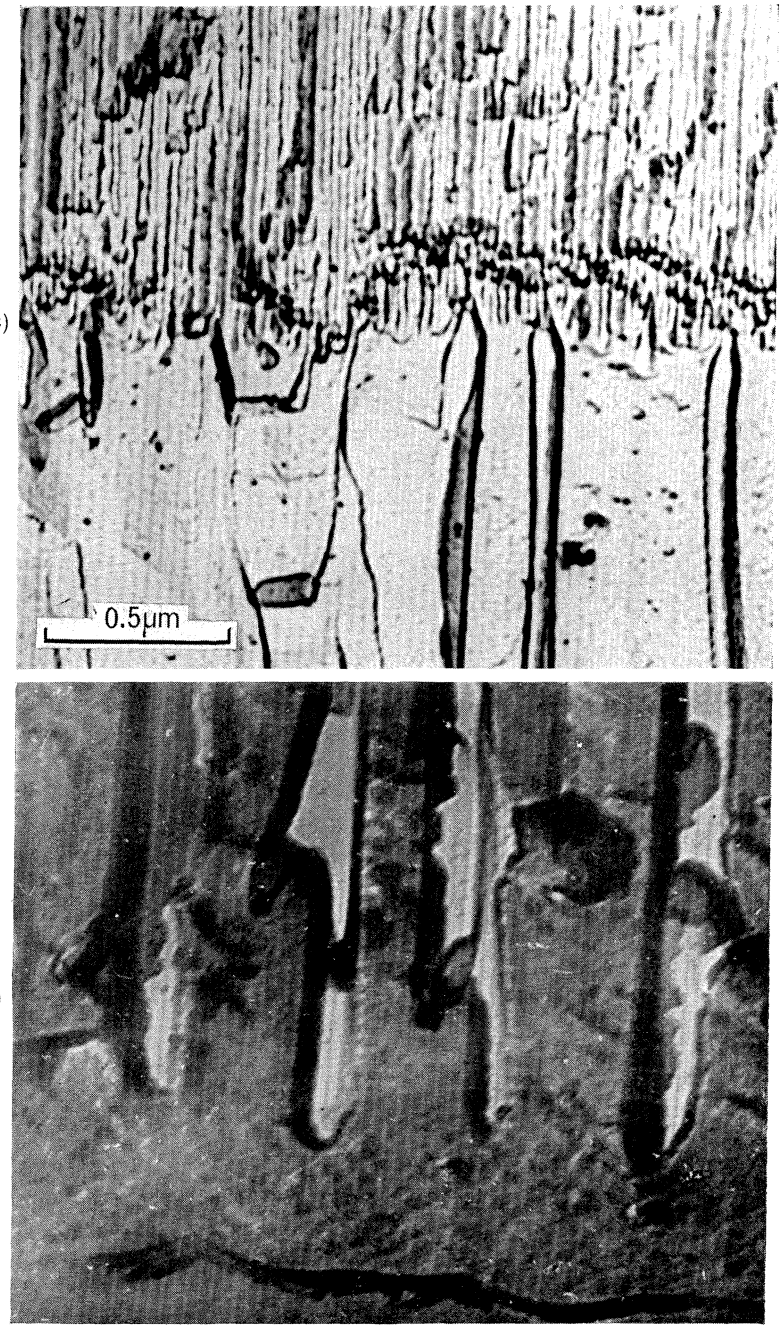

FIGURE 11. Electron micrographs of sections of 'duplex films'. (*a*) Initial formation at 18 V in 1.5 M sulphuric acid at 20 °C; reanodized at 100 V in 0.4 M phosphoric acid at 20 °C. (*b*) Initial formation at 100 V in 0.4 M phosphoric acid at 20 °C; reanodized at 260 V in 0.17 M ammonium tartrate solution (pH 7.0) at 20 °C.

Downloaded from rspa.royalsocietypublishing.org on February 28, 2013

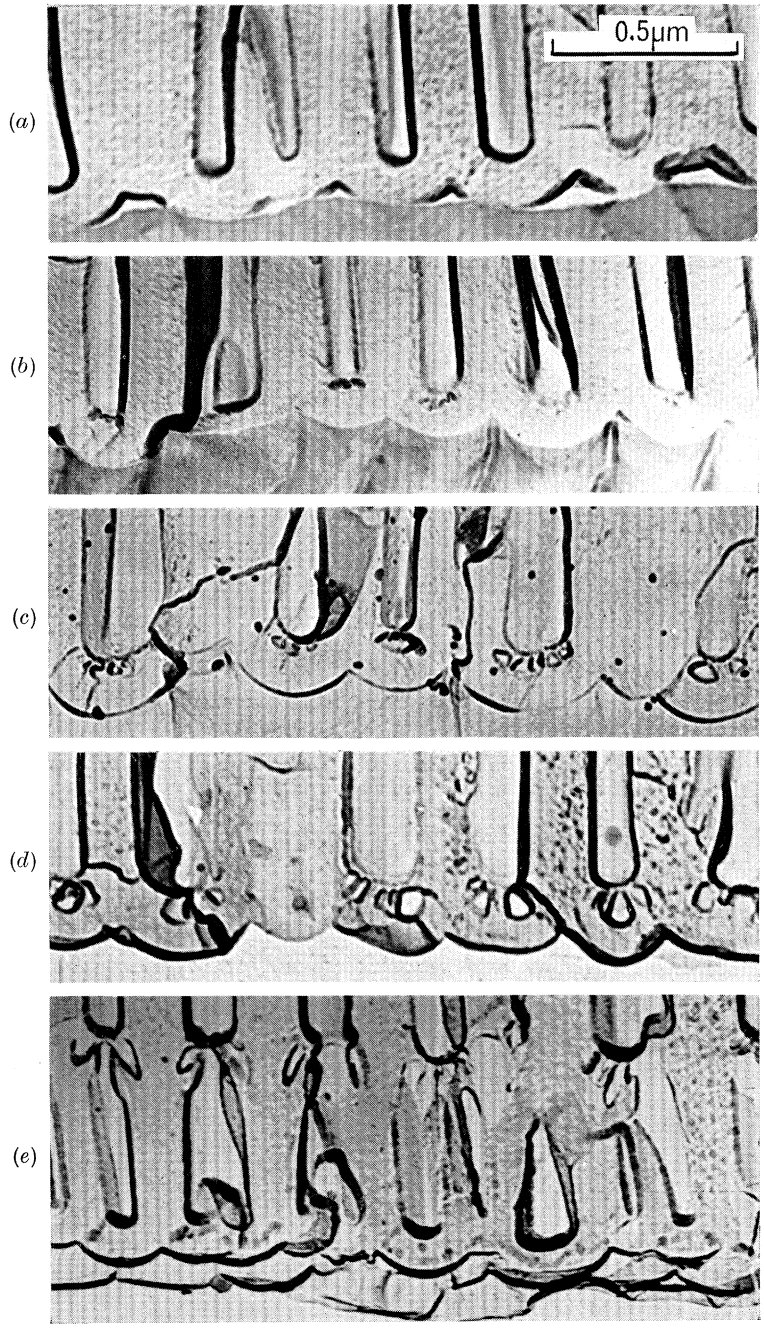

FIGURE 13. Electron micrographs of the sections of films at various times after a sudden voltage drop from 115 to 85 V in 0.4 M phosphoric acid at 25 °C: (*a*) 1 min, (*b*) 5 min, (*c*) 7 min, (*d*) 9 min and (*e*) 13 min after the change.

Downloaded from rspa.royalsocietypublishing.org on February 28, 2013

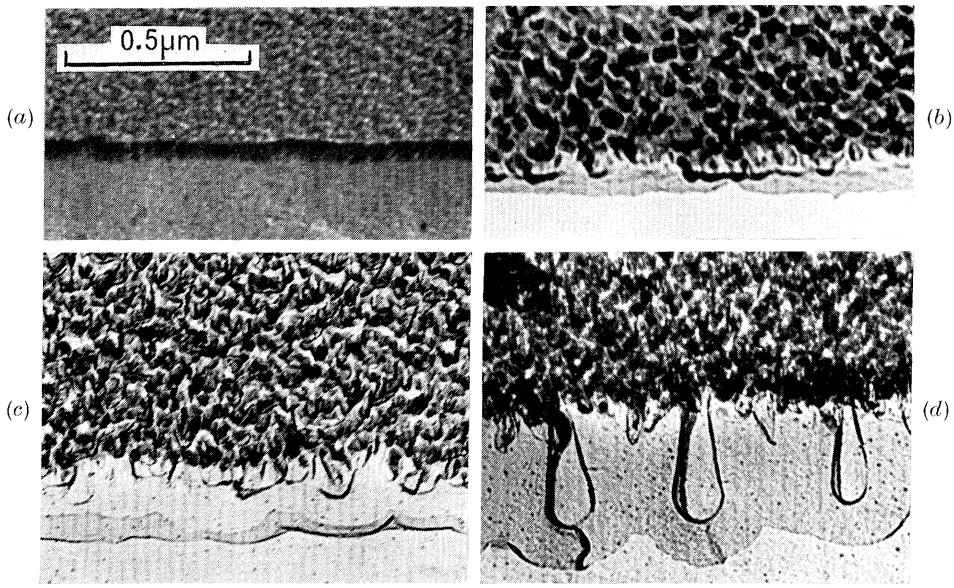

FIGURE 4. Replica electron micrographs of surfaces and sections of films grown at 50 A m^{-2} in 0·4 M phosphoric acid at 25 °C for (*a*) 40 s, (*b*) 80 s, (*c*) 200 s, and (*d*) 280 s, showing pore initiation and widening of pore diameter with increasing voltage.

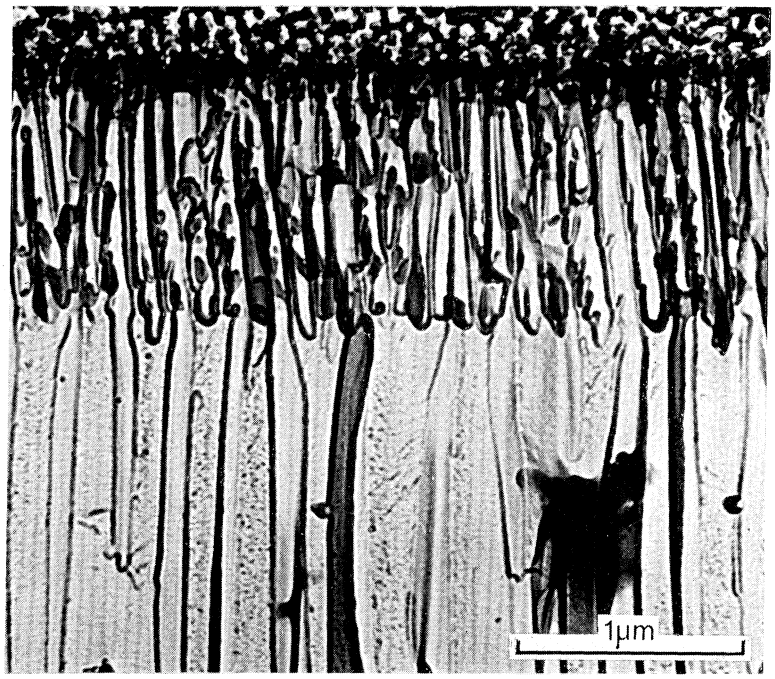

FIGURE 15. Electron micrograph of the section of a film grown in 0.4 M phosphoric acid at 25 °C for 30 min at 85 V, followed by 20 min at 115 V.

Downloaded from rspa.royalsocietypublishing.org on February 28, 2013

although across BB a different pore diameter would be expected due to the irregular fracture. Only CC would give a wrong apparent cell diameter, when measured between pore centres, because cleavage does not occur through adjacent pores. Error due to the different fracture planes observed was minimized by careful choice of even cleavage areas when measurements were made. It was generally evident that few complete fractures of the type BB or CC in fact occurred. Insufficient fracture sections were available to warrant a semi-statistical treatment of the results. This was, however, possible with measurements on film surfaces, the main error in this case being that the surface did not entirely reflect the steady-state morphology in all cases, as seen later.

Figure 1*c* shows that the pores usually extended throughout the film from the barrier layer to the outer surface, pore cessation, division or merging being relatively rare under steady-state conditions. In a plan view of the outer film surface (figure 1*d*), the pores had a wide range of diameters (70 to 240 nm) and were approximately circular. The diameters appeared to alter with depth through the film, probably partly due to the mode of fracture, although some readjustment in diameter (as explained in § 3*b*) is expected next to the outer surface. The pores were not completely close-packed, which may explain the variation in their diameters and their irregular shape in plan. Examination of the metal after oxide removal also revealed some irregularity in cell packing, although the cells were approximately hexagonal and the scalloped nature of the metal can be seen (figure 1*e*).

No variation in texture of the inter-pore oxide was detectable for these relatively mild anodizing conditions in the electron micrographs, either through the thick porous layer or in the vicinity of the barrier layer. Certainly no change in texture across the barrier layer was observed. Examination of fracture sections of films directly in a scanning electron microscope proved difficult, due to charging up of the oxide in the electron beam and the closeness to the limits of resolution, and no additional features were apparent.

Figure 2*b* shows schematically how cell and barrier layer dimensions were estimated from fracture section replicas and pore dimensions from surface replicas. The shaded portions represent the dark areas of the carbon replica due to its shape and the shadowing. In measuring barrier-layer thickness, cell-wall thickness and cell diameter, these dark areas were not included, because they represent carbon deposited on the outside of the oxide section. In measuring pore diameter from film surfaces or sections, however, they were included because they represent carbon deposited inside the pore. Using the travelling microscope directly on the plates, measurements could be made within ± 1 nm.

When barrier layer and cell dimensions were measured, forty separate estimates of each were made from the film sections and mean values taken. Whenever pore diameters were measured on film surfaces, however, 400 measurements were made, since the pore diameters showed a larger variation than the former two quantities, as noted earlier. The peak of the distribution curve of pore diameters, which was always normal, was taken as the pore diameter under these conditions.

Downloaded from rspa.royalsocietypublishing.org on February 28, 2013

(*b*) *Pore initiation*

Anodizing at constant voltage was inappropriate, due to the film thickening too rapidly because of the large initial current surge, so specimens were anodized at $50\,\mathrm{A\,m^{-2}}$ and examined at appropriate points on the voltage–time transient of figure 3*a*. The barrier-layer thickness showed a similar trend with time, rising to a maximum of 120 nm before thinning to about 80 nm (figure 3*b*). The cell and pore sizes and distributions (measured from sections) also rearranged during these periods of rising and steadying voltage until steady-state values were achieved (figure 3*c* and *d*). The direct measurements from film sections were difficult during the first 120 s of anodizing but were justified by the relatively large changes occurring. The maximum pore diameter was measured during this time, because the pores had a 'peardrop' shape in section, as seen later.

After 40 s the film surface appeared to reproduce the electropolished metal surface and show many additional minor irregularities, but no large pores were visible in section (figure 4*a*, plate 12). After 80 s, however, more surface roughening and incipient pores were apparent on the surface and in section (figure 4*b*). The voltage at this point was 90 V and still rising, so some pore initiation was occurring well before the voltage reached its maximum value. Further pore growth beneath the film surface did not appear to affect the subsequent surface topography itself greatly (figure 4*c*, *d*). Figure 4*c* illustrates preferential pore growth after 200 s, the pores developing a 'peardrop' shape in section as they increase in diameter with film thickness and with the elimination of some incipient pores. The cell and pore structures almost reached their stable, steady-state configuration after 280 s (figure 4*d*). Thus, as the voltage rose, many of the numerous initial or incipient pores ceased to function owing to the increased barrier-layer thickness, and hence cell diameter, and the remaining pores, also increased in diameter. Any exact relation could not be readily checked during this approach to the steady state.

Transmission electron micrographs after corresponding times were equally illuminating. After 40 s (figure 5*a*, plate 8) the film was again relatively structureless except for black spots about 20 nm in diameter, representing locally thick film regions. Their apparent population increased from $4.6\times10^{8}\,\mathrm{mm^{-2}}$ after 40 s to $9.0\times10^{8}\,\mathrm{mm^{-2}}$ after 80 s (figure 5*b*). After about 120 s these small nuclei began to merge, leaving areas of locally thin oxide between them (figure 5*c*), these regions probably corresponding to the small pores observed on the film surface and section replicas. The larger pores were beginning to increase in diameter after 160 s (figure 5*d*), the voltage now being almost at its maximum level. The regions surrounding these major pores look dark because the scalloped nature of the barrier layer in this location means that a thicker region of oxide is being traversed by the electron beam. As considered later, it could also be that local heating caused by current concentration here produced a higher $\mathrm{nm\,V^{-1}}$ ratio in this region of the barrier layer. The final pore structure was still establishing itself after 200 s (figure 5*e*) and 280 s (figure 5*f*), being complete after 330 s (figure 5*g*). During the

Downloaded from rspa.royalsocietypublishing.org on February 28, 2013

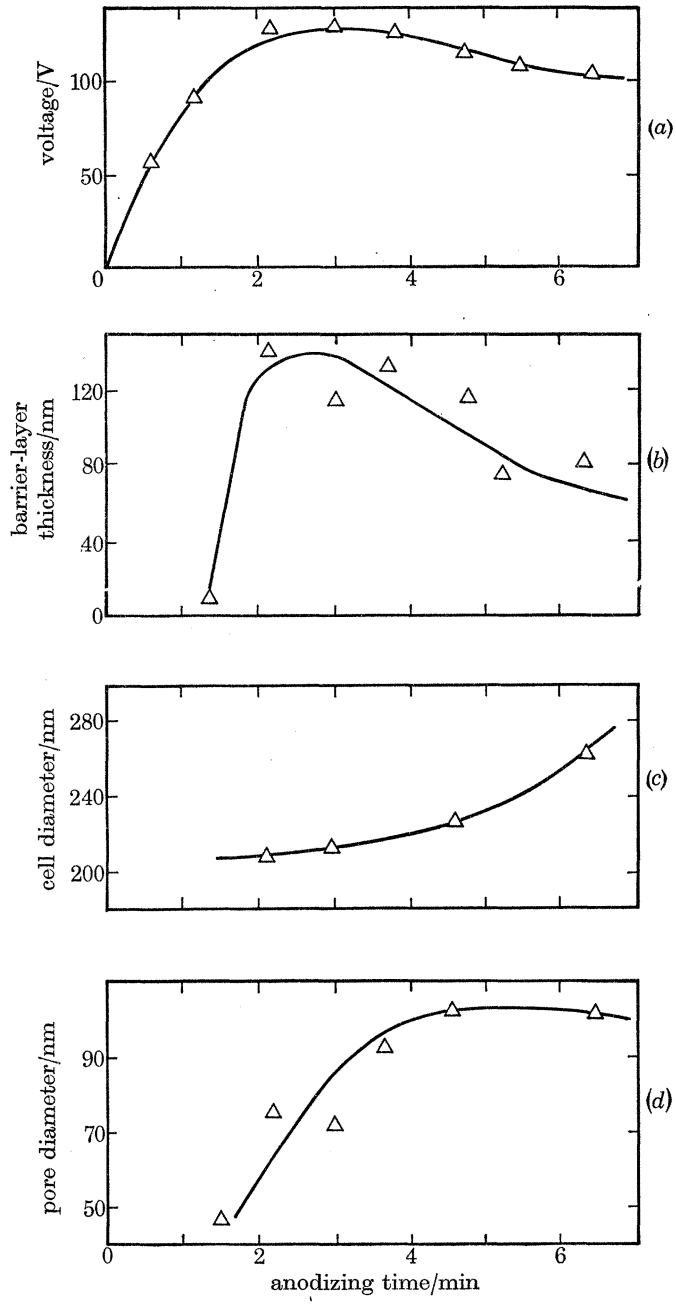

FIGURE 3. Pore initiation during anodizing at 50 A m^{-2} in 0.4 M phosphoric acid at 25 °C: (*a*) voltage, (*b*) barrier-layer thickness, (*c*) cell diameter and (*d*) pore diameter versus time. (*b*), (*c*) and (*d*) were measured from sections.

Downloaded from rspa.royalsocietypublishing.org on February 28, 2013

final period, when the larger pores were developing, the number of 'pores' (defined as any locally thin region of oxide), decreased from 0.97, 0.46, 0.26 to 0.23×10^8 'pores' mm^{-2} after 160, 200, 280 and 330 s respectively. This meant that, as the main porous structure established itself and thicker oxide grew around the main pores, the incipient 'pores' became obliterated in the transmission electron micrographs due to the thick oxide beneath them, although they were still actually present in the film. Preferential development of the larger pores and their surrounding cells occurred along metal subgrain boundaries (figure 5*c*).

(*c*) *Variation of film properties with anodizing voltage*

Films were formed at various constant voltages in the range 80 to 120 V for 1 h in 0.4 M phosphoric acid at 25 °C. Figure 6*a* shows the linear variation of the barrier-layer thickness with voltage, the nm V^{-1} ratio being 1.04. Similarly, figure 6*b* presents the variation of cell diameter with anodizing voltage, estimated from both

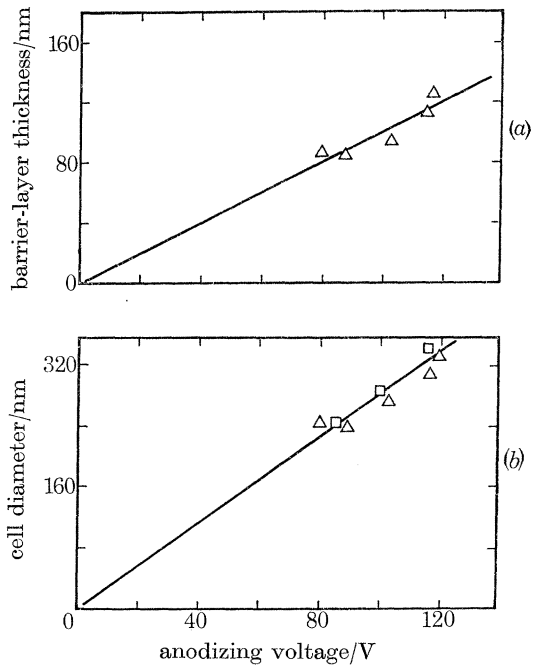

FIGURE 6. (*a*) The variation of barrier-layer thickness (measured from film sections) with anodizing voltage. (*b*) The variation of cell diameter with anodizing voltage. △, measured from film sections; □, measured from film cell-base patterns.

film sections and the cell base pattern on the metal. In the latter case the cell diameter quoted corresponds to the escribed circle of the hexagonal cell. This value is about 13 % greater than the diameter of the inscribed circle, and indeed the calculated values were slightly higher than those measured from film sections. Figure 6*b* yields a nm V^{-1} ratio of 2.77 for the variation of cell diameter with voltage.

Downloaded from rspa.royalsocietypublishing.org on February 28, 2013

Hunter & Fowle (1954*a*) found 1.19 nm V^{-1} for the barrier layer by an electrical method and Keller *et al.* (1953) found the cell diameter to increase at 2.2 nm V^{-1}.

Measurements of the cell-wall thickness indicated that it was always 0.71 of the barrier-layer thickness under these conditions for the range of cell voltages used. Thus, the pore diameter is given by

$$p = c - 2 \times 0.71d, \tag{1}$$

where p is the pore diameter, d the barrier-layer thickness and c the cell diameter. But, $c = 2.77\,V$ and $d = 1.04\,V$, expressed in nm where V is the voltage; hence

$$p = 1.29\,V. \tag{2}$$

Thus the ideal pore diameter, calculated from the other cell dimensions, is proportional to the forming voltage. The relationship probably varies somewhat with anodizing conditions, although it was confirmed approximately in experiments described in § 3*d* in which the acid concentration and temperature were varied.

Relations (1) and (2) mean that films grown at different voltages under otherwise similar conditions have the same porosity, neglecting any effects of subsequent pore widening by the prolonged contact of the porous oxide with the electrolyte. This follows because the cross-sectional area of the pore $\frac{1}{4}\pi p^2$ is proportional to V^2, while the pore population is inversely proportional to V^2. The figures obtained under the present conditions yield a porosity of 21.3 %. Pore diameters measured on outer film surfaces show a wide scatter (figure 1*d*), with the ideal pore diameter lying within the scatter limits.

Using the relationships just derived, typical dimensions for a 100 V film formed under the standard conditions are shown in figure 7. Assuming that the pore base and cell base are semi-spherical, with the same centre of curvature (figure 1*a*), θ in figure 7 is given by $\cos^{-1} 0.71$ (as a result of the observed constant relation between cell-wall thickness and the barrier-layer thickness). However, $\cos\theta$ also equals the ratio of the pore radius (r) to the radius of curvature of the pore bottom (b). Thus, for a 100 V film, the radius of curvature of the pore base is 90 nm and the corresponding radius of curvature of the cell base is 194 nm.

Comparing the new data with those of Keller *et al.* (1953) for a 120 V film, there is reasonable agreement over barrier-layer and cell-wall thicknesses but they obtained a much higher radius of curvature of the cell base (300 nm) and their (wrongly) extrapolated value for the pore diameter of 33 nm is much smaller than the present directly measured values. The main new finding is that the pore diameter, and indeed all the pertinent parameters, are directly proportional to the voltage. Apart from direct observation of steady-state films, the effect is clearly evident in the transmission electron micrographs and in the 'peardrop'-shaped pores seen in this sections. This considerably simplifies the situation and allows a simple, integrated model of film growth to emerge. Actually, careful scrutiny of the micrographs of Keller *et al.* (1953) does reveal a tendency for the pore diameter to depend upon the voltage.

Downloaded from rspa.royalsocietypublishing.org on February 28, 2013

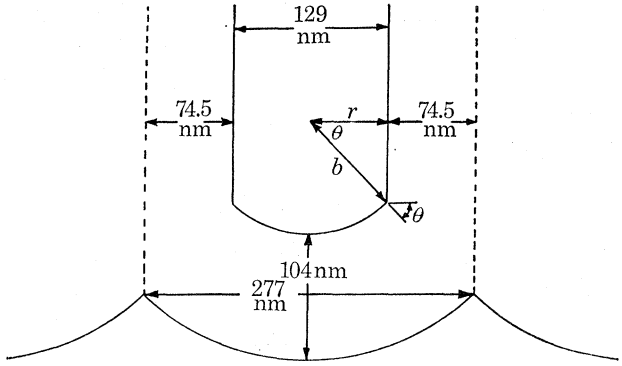

FIGURE 7. Schematic diagram of the barrier layer, pore and oxide cell of a 100 V film. r = pore diameter; b = radius of curvature of pore base;

$$\theta = \cos^{-1}\left(\frac{\text{pore radius}}{\text{pore base radius of curvature}}\right) = \cos^{-1}\left(\frac{\text{cell-wall thickness}}{\text{barrier-layer thickness}}\right).$$

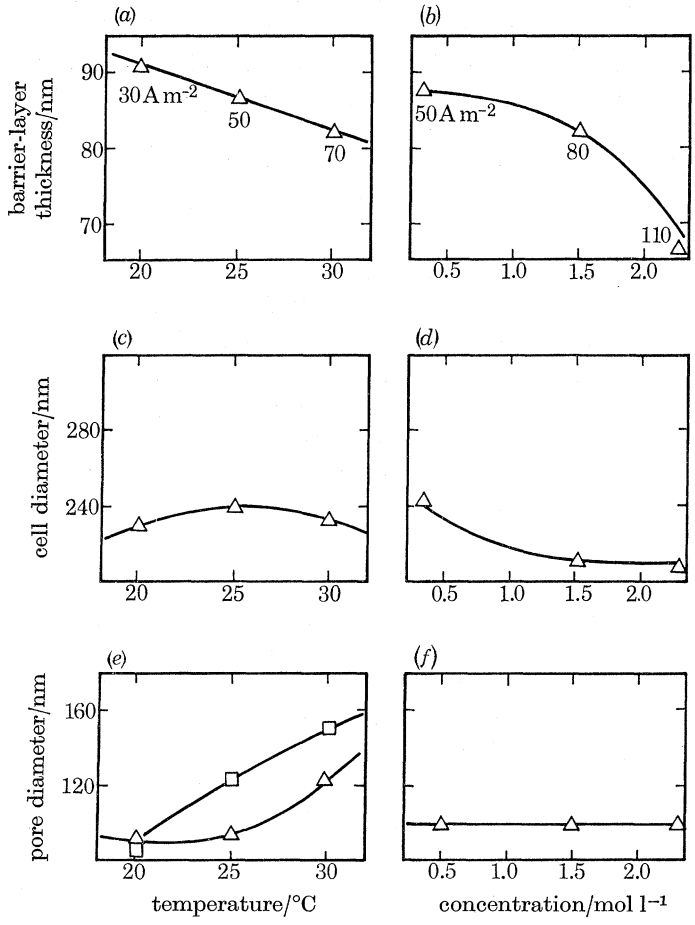

FIGURE 8. The variation of film parameters with acid temperature and concentration for constant voltage anodizing at 80 V. (*a*), (*c*) and (*e*) show the variation with temperature in 0.4 M acid; (*b*), (*d*) and (*f*) the variation with acid concentration at 25 °C. △, Measured from film sections; □, measured from film surfaces.

Downloaded from rspa.royalsocietypublishing.org on February 28, 2013

(*d*) *Variation of film properties with electrolyte concentration and temperature*

These experiments were conducted in two parts, in which anodizing under similar conditions was performed at constant voltage and constant current density respectively.

At constant voltage, films were formed for 1 h at 80 V in 0.4 M phosphoric acid at 20, 25 and 30 °C respectively, and also in 1.5 M and 2.5 M acid at 25 °C. The barrier-layer thickness fell slightly as the conditions became more aggressive with rising temperature, the current density established rising accordingly (figure 8*a*). Increasing acid concentration, over the ranges examined, had a much greater effect on the barrier layer than temperature, the measured value falling from 87 nm in 0.4 M acid to 67 nm in 2.5 M acid (figure 8*b*). Little variation of cell diameter, as measured from sections, was detectable with temperature (figure 8*c*), although the fall from 240 nm in 0.4 M acid to 210 nm in 2.5 M acid may have been significant (figure 8*d*).

Pore diameters, measured in section at their base, showed some increase with temperature (figure 8*e*), but a bigger increase occurred at the film surfaces, due to chemical dissolution at the outside of the film. Pore diameters showed little variation with increase in acid concentration when measured on film sections (figure 8*f*). This observation confirms the point made previously that pore diameters measured in section must be treated with reservation. Unfortunately no surface measurements were possible due to obliteration of the pores by bulk dissolution there.

In the corresponding constant current density experiments, films were grown for 1 h at 100 A m^{-2}, the voltage being allowed to take up its natural value. The barrier layer thinned from 130 nm at 20 °C to 100 nm at 30 °C (figure 9*a*). Acid concentration again had a greater effect (figure 9*b*), reducing the barrier-layer thickness from 100 nm in 0.4 M acid to 30 nm in 2.5 M acid. These effects were in agreement with the voltages taken up, since the barrier-layer thickness is approximately proportional to the voltage. The changes were reflected in the variations of cell diameter, and in this case pore diameter from sections, with voltage (figure 9*c* to *f*). Pore diameters at the surface were again larger than next to the barrier layer. The pore diameters measured on film sections reinforced the conclusion that the pore diameter is directly proportional to the formation voltage, although the constant of proportionality would be expected to vary slightly with the anodizing conditions.

Electron micrographs of film surfaces clearly showed pore widening at the outer surface upon increasing the temperature and pore merging and eventual irregular bulk dissolution upon increasing the acid concentration. For example, figure 10*a*, plate 9, shows some effect of bulk dissolution in the outer regions of a film formed in 2.5 M acid at 25 °C, although the depth of action was usually much less under milder conditions (figure 1*c*). Figure 10*b* shows the surface of a film where pore widening was the major process (compare with figure 1*d*) whereas figure 10*c* shows where bulk attack obliterated the porous morphology.

Downloaded from rspa.royalsocietypublishing.org on February 28, 2013

(e) *Variation of film properties with electrolyte type*

Various experiments were performed in which films formed in electrolytes giving porous films were transferred to electrolytes giving barrier films and vice versa. Transfers of specimens between various acids giving porous films were also conducted. In general, anodizing could be continued successfully in the second electrolyte immediately, providing that the barrier layer produced in the first electrolyte was not too thick to allow passage of current in the second electrolyte.

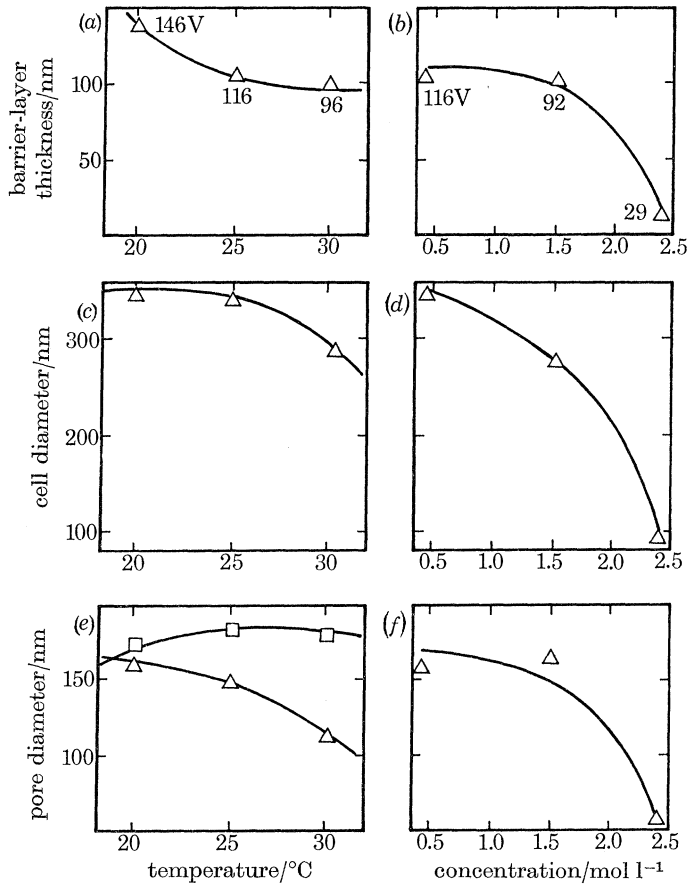

FIGURE 9. The variation of film parameters with acid temperature and concentration for constant current density anodizing at 100 A m^{-2}. (*a*), (*c*) and (*e*) show the variation with temperature in 0.4 M acid; (*b*), (*d*) and (*f*) the variation with acid concentration at 25 °C. △, Measured from film sections; □, measured from film surfaces.

Figure 11*a*, plate 10, shows a 'duplex' film grown at 18 V in 1.5 M sulphuric acid and then transferred to 0.4 M phosphoric acid and re-anodized at 100 V. Only a few pores of the first film widened and continued to grow, the funneling being clearly evident and the cell size much increased. Figure 11*b* shows the effect on the barrier layer of re-anodizing a film, grown at 100 V in 0.4 M phosphoric acid, in 0.17 M

Downloaded from rspa.royalsocietypublishing.org on February 28, 2013

ammonium tartrate solution, pH 7. Here the porous region corresponds to the 100 V anodization and the thickened barrier layer is typical of the 260 V treatment. The radius of curvature of the cell base, and presumably that of the pore base, increased during the re-anodization.

(*f*) *The influence of changing the anodizing voltage during growth*

After forming films individually at constant voltage for 30 min, the circuit was broken in each case, the voltage then being quickly adjusted to the new value to be applied, either higher or lower than the original value, the circuit completed and the specimen re-anodized at the new voltage. The current/time curves were recorded and specimens removed at appropriate stages for electron microscopical examination. Both current density and time on the curves presented were reproducible to within 5 %.

Figure 12*a* shows that, upon dropping the voltage from 115 to 85 V, there was a reproducible period of low current in the range 1 to 2.5 A m^{-2}. From figure 12*b*, presenting barrier-layer thicknesses measured directly in section, it is evident that barrier-layer thinning commenced immediately after the voltage was lowered. The scatter in barrier-layer thickness in these experiments was greater than usual because time was an added variable but the results shown, and numerous others not plotted, indicated an indisputable trend. Figure 12*c* shows the corresponding changes in cell and pore diameters, measured from film sections, the technique being reasonably valid here for pore diameter because of the large changes involved.

The sequence of section micrographs in figure 13, plate 11, shows that the initiation of new pores at the pore bases only occurred when the current began to rise after the induction period. From each original pore several small pores nucleated and increased in diameter until certain of them ceased to function, leaving the new equilibrium number of pores characteristic of the second, lower, anodizing voltage. Figure 12*b*, *c* shows that the main pore size remained virtually constant until the new pores initiated over the whole pore base after 300 to 360 s, the new pores then increasing in diameter to a value in nm corresponding to 1.29 × the applied voltage, as determined in § 3*c*. Cell diameters also remained constant until after 300 to 360 s but slight changes then began to occur in curvature of the cell bases which were reflected in the cell diameter measurements and correspond to growth of fresh oxide via the new porous system.

In order to confirm that barrier-layer thinning during the recovery time was due to 'field-assisted dissolution' (possibly thermally enhanced due to local heating), not simple 'chemical dissolution', separate experiments were performed. The first set consisted of measuring the recovery times (i.e. time after the voltage drop to resume the new steady-state current) (reproducible to within 10 %) for various voltage drops imposed during anodizing, the results being given in table 1. In the second set of experiments the same voltage drop was applied in each case, but the specimen was left in the anodizing electrolyte for various times after breaking the circuit and before the new cell voltage was applied. The recovery times are recorded

Downloaded from rspa.royalsocietypublishing.org on February 28, 2013

in table 2. Although slow chemical dissolution occurred regardless of whether the field was applied or not, barrier-layer thinning was markedly dependent on the field and occurred quicker at higher fields.

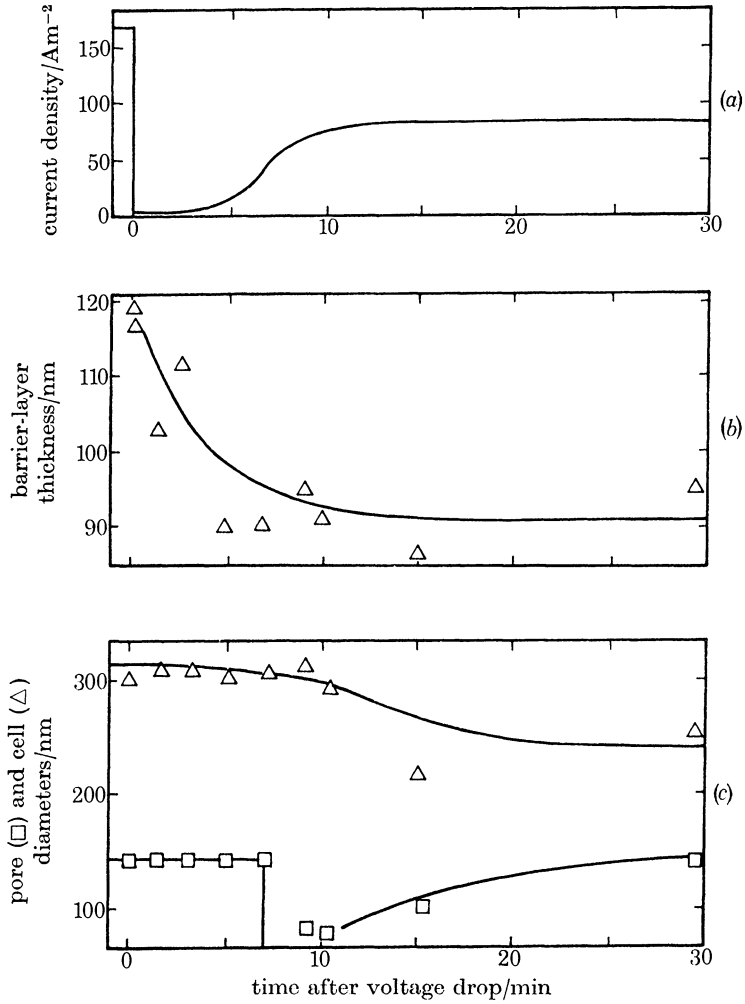

FIGURE 12. The effect of a sudden drop in the constant anodizing voltage from 115 to 85 V in 0.4 M phosphoric acid at 25 °C upon (*a*) current density, (*b*) barrier-layer thickness and (*c*) pore and cell diameters, measured from film sections. △, Cell diameter; □, pore diameter.

When the cell voltage was raised from 85 to 115 V in reverse experiments, after the initial current surge, which was limited by the power output of the anodizing unit, the current density fell reproducibly to a minimum and then rose to the current density characteristic of the new cell voltage within 180 s of the initial voltage rise (figure 14*a*). Figure 14*b*, giving barrier-layer thickness measured directly from sections, shows clearly that the thickness rose to 116 nm after 60 s,

Downloaded from rspa.royalsocietypublishing.org on February 28, 2013

TABLE 1. THE VARIATION OF RECOVERY TIME WITH VOLTAGE DROP

initial voltage/V	final voltage/V	voltage drop/V	recovery time/s
115	95	20	75
115	85	30	390
115	75	40	1410

TABLE 2. THE VARIATION OF TOTAL RECOVERY TIME AND RECOVERY TIME WITH APPLIED FIELD FOR VOLTAGE DROP FROM 115 TO 85 V

time without field/s	total recovery time/s	total time − time without field/s
180	507	327
300	630	330
600	870	270

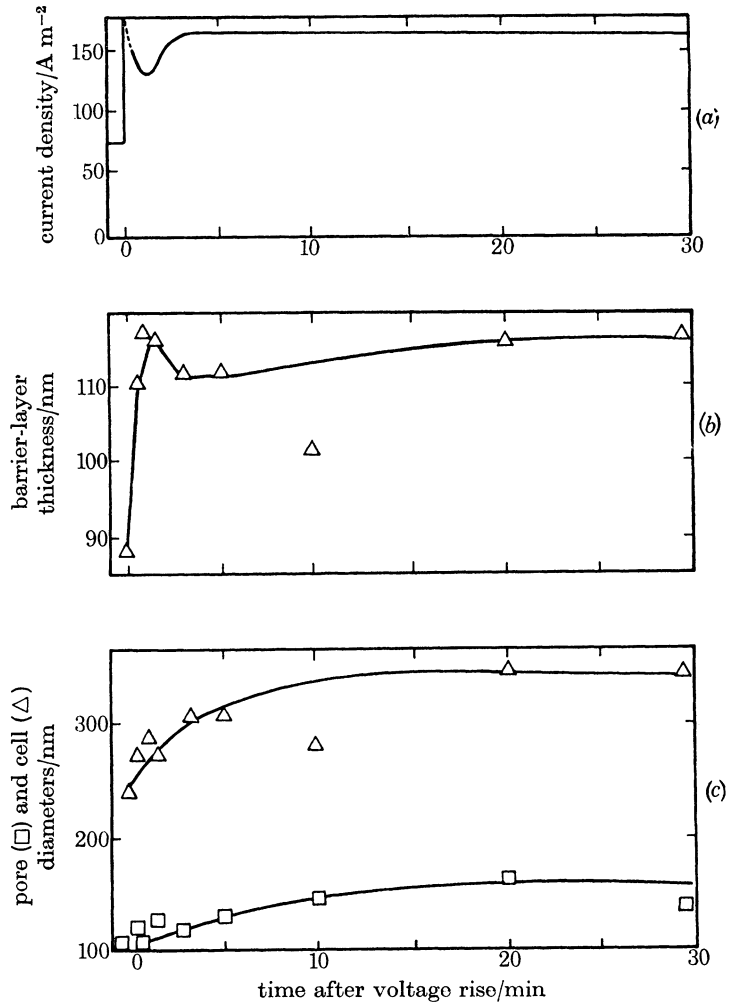

FIGURE 14. The effect of a sudden rise in the constant anodizing voltage from 85 to 115 V in 0.4 M phosphoric acid at 25 °C upon (*a*) current density, (*b*) barrier-layer thickness and (*c*) pore and cell diameters, measured from film sections. △, Cell diameter; □, pore diameter.

Downloaded from rspa.royalsocietypublishing.org on February 28, 2013

this time corresponding to the minimum in the current density–time curve. The barrier layer then fell to its new steady-state thickness after 180 to 240 s. Figure 14*c* shows that the cell and pore diameters, measured from sections, took much longer (at least 600 s after the voltage change) to reach the steady-state values.

The changes observable in porous film morphology visible in fracture sections were generally rather more subtle than when the voltage was dropped. Since the voltage, and thus the equilibrium cell diameter, were larger after the voltage increase, less cells and pores could be accommodated per unit area, and so some pores were eliminated. This process was occasionally easily seen (figure 15, plate 12).

4. Discussion

(*a*) *General film morphology and structure*

The geometrical model of Keller *et al.* (1953) has been confirmed in principle but not in several important details. The major criticism of their study is that it was not appreciated that the pore diameter, the cell diameter and the barrier layer thickness are interrelated and all proportional to the formation voltage, this requiring a major modification of theories of film formation. No evidence has been found for their star-shaped pore sections and the regularity in pore and cell size, and in the close-packed hexagonal packing of cells, is not as great as they claimed. There is little evidence of pore widening in depth due to prolonged contact with the electrolyte, pores generally being 'trumpet-shaped' under moderately severe conditions. This is due to increased chemical dissolution of the pore walls at the outer surface, where the Al^{3+}-enriched solution in the pores can be readily exchanged by unsaturated bulk solution. Only in very concentrated electrolyte does this pore opening effect penetrate relatively deeply into the film and significantly thin the entire film. Major dissolution within the porous structure, therefore, usually only occurs near the pore bases in the presence of the field.

Limited support for the concept of bundles of hollow fibres (Ginsberg & Wefers 1963; Csokan 1964) in the film may be recognized but these are merely cells and pores in the outer parts of the film which become distorted by aggressive electrolytes. Slight tilting of the pores and cells from the normal to the macroscopic surface (Franklin & Stirland 1963) was not observed and must be related to formation on a slightly faceted surface linked to the surface preparation. No evidence has been found for the proposal of Murphy & Michelson (1962) that the regular pores play no major role in the formation process. However, infrared spectroscopy studies (O'Sullivan, Hockey & Wood 1969), on films formed in sulphuric acid, indicate that the inter-pore material consists of fine microcrystallites of largely anhydrous alumina joined by intercrystallite regions containing molecular water, hydroxyl groups and probably the acid anion. The aluminium oxide has ionic properties, but with some covalent character (Wells 1952; Wood & Pearson 1967; Vijh 1969; Syrkin & Dyatkina 1950), so it is likely that there is some short range order within the oxide,

Downloaded from rspa.royalsocietypublishing.org on February 28, 2013

to an extent depending upon the anodizing conditions, favouring some of the concepts of Dignam (1965) and Murphy & Michelson (1962). The intercrystallite surfaces, although important in post-anodizing treatments, are a by-product of the anodizing reaction not a cause of the unique film morphology.

The present model predicts that the microcrystallites are relatively close-packed in the barrier layer of porous films, the surfaces between them containing acid anions and OH^- ions built in during formation, but being relatively inaccessible to the electrolyte during normal anodizing conditions. Under more severe conditions more anion and OH^- ion tend to be incorporated into the barrier layer, leading to slightly more extensive and 'open' intercrystallite surfaces. The effect cannot, however, be large because although the ionic conductivity of the barrier layer and formation field change significantly they do not depend greatly on acid type or conditions. The extent of inorganic anion incorporation into barrier layers has been studied (Rogers, Draper & Wood 1968), as indeed has OH^- ion and proton incorporation in the presence of a field, leading to varying degrees of pore initiation, sponginess and solubility at the outside of the barrier layer (Brock & Wood 1967). Because of the greater contact time with severe acid, the inter-pore regions in the outer parts of the porous film become progressively more open and spongy, due to the enlargement of the intercrystallite regions, causing cracking and film collapse in extreme cases during drying out (O'Sullivan 1968). The attack of the acid manifests itself in this way, rather than by uniform enlargement of the pores within the film. Electron microscopy tends to reveal these substructural changes in the more severely exposed regions but in no detail in the barrier layer. This does not, of course, preclude the possibility of chemical variations across the barrier layer and indeed the entire film.

(*b*) *Barrier-layer growth*

Although the present paper is concerned largely with porous films, barrier-layer growth must be considered slightly more deeply, before introducing the complications of pore initiation and growth. Despite elegant marker experiments indicating counter-migration of Al^{3+} ions and oxygen-containing anions (relative transport numbers being 0.72 and 0.28 for cation and anion respectively in aqueous electrolyte at 100 A m^{-2}) (Davies, Domeij, Pringle & Brown 1965), the mechanism of migration is still uncertain (Amsel, Cherki, Feuillade & Nadai 1969). Although it is often tacitly assumed that single ions either move right through the film under the field or else make single jumps in the 'amorphous' material, the nature of movement is relatively unproven (Dignam 1965; Brock & Wood 1967) and it is not clear how much transport is through the crystallites and how much through the intercrystallite regions. Such matters are really crucial in determining where new material is deposited and in deciding how incipient pores nucleating on the outside of a film develop into steady-state pores. The experiment in which the barrier layer of a porous film was thickened in a neutral electrolyte, increasing the cell and pore base radii of curvature (see § 3*e*), at first sight favours considerable anion movement, but subtle, local field changes during the re-establishment of equilibrium in the scalloped

Downloaded from rspa.royalsocietypublishing.org on February 28, 2013

pore base should perhaps not be discounted. Certainly mere pore filling is not the only process.

The evidence suggests that some of the migrating anions are OH^- ions (Hoar & Mott 1959; Vermilyea 1963; Heine & Pryor 1963; Brock & Wood 1967), the remainder being O^{2-} ions (Davies *et al.* 1965; Brock & Wood 1967) or oxyanions from the acid (Hoar, Mears & Rothwell 1965; Rogers *et al.* 1968). There appears to be a concentration gradient of OH^- ions and oxyanions through the barrier

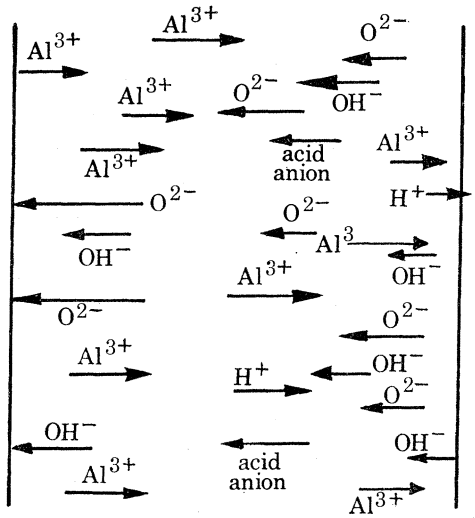

FIGURE 16. Schematic representation of the distributions and directions of movement of ions through the barrier layer during film growth.

layer, with enrichment towards the outer surface. If we assume a corresponding reverse distribution for cations, the distribution of charged species is as shown schematically in figure 16 (the main 'lattice' having been omitted for simplicity). The relative proportions of the three anions migrating depend on the relative ease of discharge of ions under the local conditions at the oxide/electrolyte interface and upon their charge and size. O^{2-} ions and oxyanions would remain unchanged within the film but OH^- ions could be converted into O^{2-} ions with the release of a proton upon taking their place in a local film configuration. The proton might be expected to migrate quickly out of the film under the high field (Hoar & Mott 1959; Vermilyea 1963), and thus not contribute significantly to any positive space charge. Such proton-portering processes and indeed OH^- migration itself, are not essential to the mechanism of film growth but it is entirely reasonable that OH^- ions (0.153 nm) should enter the barrier layer, because they are only slightly larger than O^{2-} ions (0.140 nm) (Wells 1952). Residual hydroxyl ions trapped within the film lead to its established hydrogen-bonded structure, with an increase in OH^- content towards its outer surface. This effect is greater at high pH (Brock & Wood 1967), probably due to the increased number of OH^- ions capable of competing with PO_4^{3-} ions and water molecules for adsorption and with O^{2-} ions for entry into the film.

Downloaded from rspa.royalsocietypublishing.org on February 28, 2013

The O^{2-} or OH^- ions for film formation could originate from water, or in certain cases from the acid anion. Traces of water are often necessary for anodizing, in non-aqueous solutions. The anodizing of aluminium usually only occurs in acid electrolytes containing divalent or trivalent anions. Significantly, such acids can form more than one anion by removal of successive protons from the acid molecule:

$$H_3PO_4 \rightarrow H^+ + H_2PO_4^- \rightarrow H^+ + HPO_4^{2-} \rightarrow H^+ + PO_4^{3-}$$

or

$$H_2SO_4 \rightarrow H^+ + HSO_4^- \rightarrow H^+ + SO_4^{2-}.$$

Divalent or trivalent ions absorb onto the positively charged alumina surfaces more strongly than monovalent ions, the adsorption being even stronger under the influence of a high field. Furthermore, water molecules would also tend to cling to

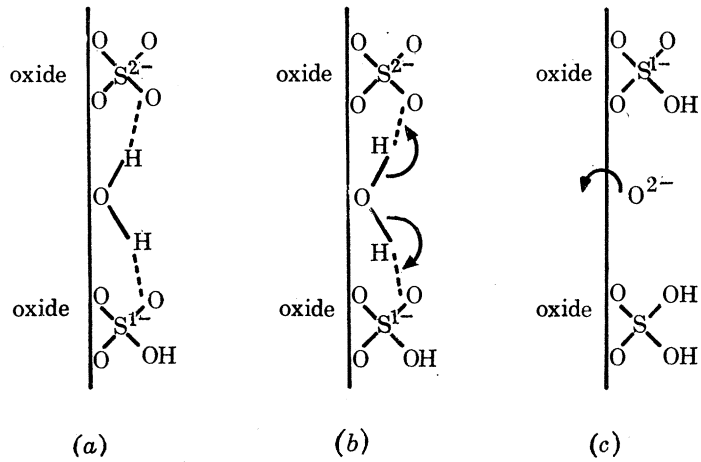

FIGURE 17. Schematic representation of the production of O^{2-} or OH^- ions at the surface of a barrier layer during growth.

film surfaces under such conditions, with the negatively charged oxygen atom next to the surface. Taking sulphuric acid for simplicity, figure 17*a* depicts the surface situation and the possibility of hydrogen bonding between hydrogen atoms of the water molecule and the oxygen atoms of the larger oxyanions. This weakens the O—H bonds of the water molecule and helps the field to remove the oxygen atom from the hydrogens (figure 17*b*). If only one hydrogen is removed the result is an OH^- ion, while removal of them both yields an O^{2-} ion. These reactions would be facilitated by the ease of conversion of the oxyanions into the ion of lower valency or even of the monovalent ion into the acid molecule. At higher fields the discharge of the larger acid anion would be expected to become more competitive. Any anions incorporated into the film might be expected to modify the oxide structure and properties and affect the dimensions of the submicrocrystallites. It is generally observed that anion incorporation into the film during chromic acid anodizing is low (probably at least partly due to the large size of the dichromate ion). Substantial quantities enter the film in sulphuric acid but only moderate amounts in phosphoric acid.

Downloaded from rspa.royalsocietypublishing.org on February 28, 2013

(c) *Pore initiation and growth*

The transmission electron microscopy of thin, stripped films shows non-uniform thickening of the barrier layer at constant current density, with apparent 'nuclei' or spots of thicker oxide (a few tens of nm in diameter) which increase in number and size until they merge eventually, leaving thin areas of oxide between them. Figure 18 attempts to display the inevitably non-uniform current distribution during this process, with initial concentration at the thickening regions but eventual concentration at the thin areas which are the precursors of the steady-state pores. Figure 18*d*

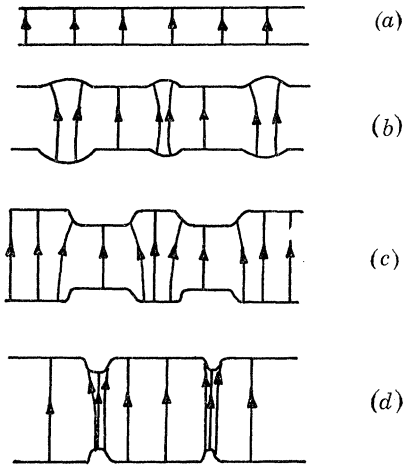

FIGURE 18. Schematic representation of irregular barrier-layer thickening and the distributions of current during pore initiation in pore-forming electrolytes.

would, of course, rapidly transform into the situation with a scalloped pore base, the film then actually penetrating more, not less, into the metal in these locations (figure 20). As the voltage rises, the pore and cell diameters increase and so a smaller number of major pores eventually propagate, certain of the incipient pores ceasing to function, and any very large ones would not grow much and might even decrease in size.

The relative importance of non-uniform growth and non-uniform dissolution in producing this morphology is not clear-cut, particularly in view of the relatively high film thickness (e.g. 50 nm at 40 s). For nominally constant current density anodizing the field should, of course, be constant over the surface. However, some local variations due to structural and impurity effects in the metal or the pre-existing air-formed film seem possible. Thus, although there appear to be too many 'nuclei' for them to be related to substrate dislocations, there is evidence that the metal substructure is involved because the main pores and cells develop most rapidly along the metal subgrain boundaries. Local thickening could be due to easier entry of ions into the film at defective sites (if metal/oxide interface control is acceptable) or to easier transport through the film (if bulk transport control is rate-determining).

Downloaded from rspa.royalsocietypublishing.org on February 28, 2013

This would be due to greater structural imperfection of the film or possibly to greater impurity at the regions. For anodizing in neutral electrolytes, the barrier-type films, although possessing a 'self-structure', do not display such irregular thickening as observed here. This is expected because localized concentration of current at thin areas will lead simply to the film thickening faster there and the production of a uniform film. However, where local dissolution, particularly in the presence of the field and possibly local heating, can occur as a competitive process, the pore is self-sustaining, as explained later. Any direct effects of the substrate would be expected to become less pronounced as the film thickened, causing the film between the main pores to become more uniform in thickness.

If the degree of crystallinity or composition of the 'amorphous' film varies locally, its dissolution rate, and possibly its growth rate under the field, might be expected to vary accordingly. It is well known that high voltages tend to promote oxide crystallinity. It is even possible that some of the contrast visible in figure 5, plate 8, is due to differences in electron capacity of the film because of such variations, particularly as the irregular nucleation pattern was not quite as evident from replicas (figure 4, plate 12).

It does not seem necessary or possible to invoke local field-inhibited, proton-induced dissolution (Hoar & Yahalom 1963) to explain the pore pattern under the present constant current density conditions. At constant voltage, a high applied voltage leads to a massive current surge initially, oxide growth far outweighing any dissolution until the growth current has fallen to a relatively low value. Pores would then initiate quickly, taking up a diameter dependent upon the constant voltage across the film. Thus the suggestion (Hoar & Yahalom 1963) that barrier-layer formation is identical in most electrolytes could well be true for constant voltage anodizing, but at constant current density some dissolution would be expected from the outset. The evolving nucleation pattern illustrated in figure 5 would be expected to vary with the electrolyte and the anodizing conditions.

The fact that films growing at 500 A m^{-2} are thickening about 5 times as fast as those growing at 100 A m^{-2}, even though the respective barrier layers stay essentially constant in thickness with time, indicates that film dissolution at the pore bases must be faster in the former case. Together with the special experiments of § 3*d*, this is a strong indication that dissolution of the film at the pore bases is field-assisted (Hoar & Mott 1959), since the electrolyte conditions are nominally identical in each case. Local Joule heating, which would be higher at higher current density, may be a contributory factor but is not thought to be the major effect. Thus, Hunter & Fowle (1954*b*) calculated that, for anodizing at 200 A m^{-2} in 1.5 M sulphuric acid at 21 °C, the actual dissolution rate at the pore bases must be 372.5 nm min^{-1}, compared with a chemical dissolution rate of 0.084 nm min^{-1} under these conditions. They estimated that this would require 53 % acid boiling at 124 °C at the pore bases to maintain dissolution at the required rate. Applewhite, Leach & Neufeld (1969) measured overheating of a 0.1 mm wire, and hence they claim of the film, by 2 to 3 K at 100 A m^{-2}, 5 to 6 K at 200 A m^{-2} and 20 K at 800 A m^{-2} for barrier type films

Downloaded from rspa.royalsocietypublishing.org on February 28, 2013

growing at 200 V in ammonium borate solutions. The temperature rise seems insufficient to be the major factor here, even allowing for local heating at pore bases, if in fact significant temperature gradients could exist in such thin films, which is doubtful. Leach & Neufeld (1969) considered that heat can play a part in enlarging pores with time under fixed formation conditions. It could also be argued that film material produced at high current density is more amenable to dissolution, perhaps due to differences in anion incorporation. Although such effects become apparent later (§ 4*d*) they appear to be of secondary importance to the massive effect of field-assisted dissolution of contaminated alumina. The steady-state pore pattern is therefore largely determined by an equilibrium between film growth and film dissolution under the field at the pore bases. It is achieved, as shown shortly, by geometrical changes in the pore base shape as equilibrium is approached.

A more precise examination of field-assisted dissolution of the film material is now appropriate. Since Al_2O_3 is considerably, but not entirely, ionic in nature, its dissolution involves the breaking of Al—O bonds in the lattice, the reaction products being $Al(H_2O)_6^{3+}$ ions and probably H_2O. Thus, any process which weakens the Al—O bonds in the oxide eases the dissolution process at kink sites by lowering the effective activation energy for dissolution. Two such processes are evident here, hydrogen bonding of the outer regions of the barrier layer and, much more important, the presence of the electric field across the oxide/electrolyte interface at the pore base. Bernal (1959) indicated that hydrogen bonding would weaken interionic bonding of this type and this would make dissolution easier. A redistribution of the electron cloud of any O^{2-} ion taking part in hydrogen bonding occurs, resulting in an effective lowering of charge on the O^{2-} ion, so decreasing the Al—O attraction. It is the OH^- ions momentarily trapped in the lattice, prior to moving on or decomposing into O^{2-} ions and protons, rather than those in the process of migrating, which could contribute most to the hydrogen bonding.

Figure 19*a* shows the oxide schematically, assumed for simplicity to have a simple NaCl structure, adjacent to the solution before the field is applied. Application of a field across the oxide (figure 19*b*) effectively polarizes the bonds in the oxide. At and close to the barrier-layer surface the Al—O bonds increase in length because the field is tending to pull the O^{2-} ions into the oxide and to push the Al^{3+} ions into solution. Solvation of Al^{3+} ions by water molecules via the activated complex, and the removal of O^{2-} ions by H_3O^+ ions, giving water, are facilitated (figure 19*c*, *d*).

It is uncertain whether during incipient pore and nucleus development the average field across the oxide at the pore bases is greater than, the same as, or less than the field across the plane regions of film, but it must eventually be greater due to current concentration at the developing major pores. The stage after the concentration of current in the initially thin oxide regions (incipient pores) of figure 18*d* is illustrated in figure 20, where just a single major pore (figure 20*a*) and then two adjacent pores (figure 20*b*) are seen developing. The lines representing the easiest current paths through the barrier layer may also be considered as the lines of force of the electric field. The configuration of these lines shows that, alth ough the field is

Downloaded from rspa.royalsocietypublishing.org on February 28, 2013

constant across the flat parts of the barrier layer, at the curved pore base it increases in passing from WX to YZ. At the pore bases the local field in the vicinity of the pore base YZ, which is the field assisting dissolution, is greater than the average field between YZ and WX which determines film growth, as suggested by Hoar & Mott (1959). Thus, the rate of dissolution near YZ is assisted by the field to a greater

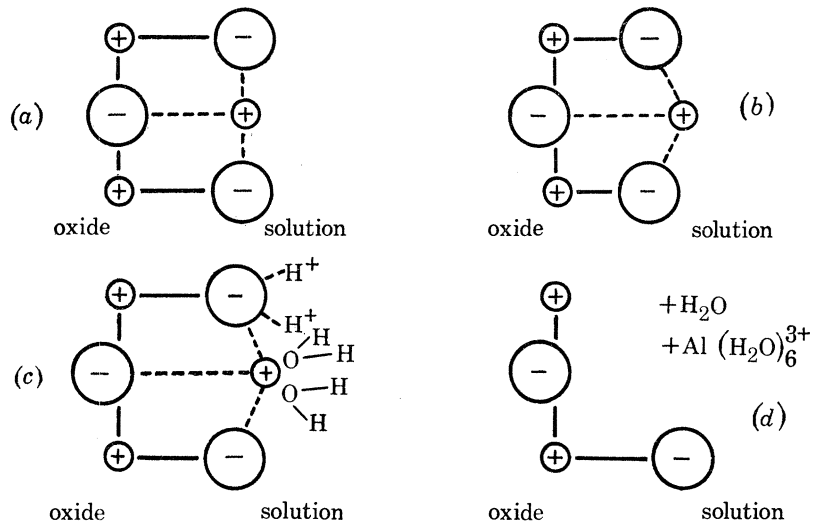

FIGURE 19. Schematic representation of the field-assisted dissolution of Al_2O_3 (*a*) before polarization, (*b*) after polarization, (*c*) removal of Al^{3+} and O^{2-} ions, and (*d*) the remaining oxide.

extent than is growth, and also more than elsewhere on the outer film surface, so that the pore can be propagated and becomes surrounded by a cell. During this period, when only occasional major pores have initiated, the rest of the film surface is still passing current, but the true current density at the major pore base is greater than elsewhere because the increased oxide dissolution here results in a lower barrier-layer thickness, and also the pore is drawing current from the larger area of the cell base. The self-sustaining nature of pores is clear. Other locally thin areas can only develop into pores if they can compete with already established pores for current. The distribution of current lines in figure 20 shows that a high forming voltage, producing a thicker barrier layer and cell wall, will require greater pore separation and fewer pores than a low voltage. It is expected that an approximately close-packed distribution will be arrived at and that this will be more regular beneath the surface than upon it, because the latter represents the initial non-steady state situation. The rate of spread of pores will depend upon the dissolving ability of the electrolyte under the field.

Any theory of porous film formation must explain why a certain constant pore diameter is attained under a given set of anodizing conditions. The initial 'peardrop' pore section shape formed at constant current density is due to two effects. First, the voltage rises progressively, so the pore diameter increases proportionately, as

Downloaded from rspa.royalsocietypublishing.org on February 28, 2013

shown earlier. Secondly, a proportion of the numerous, random, incipient pores nucleated on the outer film surface must be eliminated as the remainder take up their equilibrium distribution and size. At constant voltage, the second factor predominates, because the barrier layer is much nearer its equilibrium thickness when major pore initiation occurs.

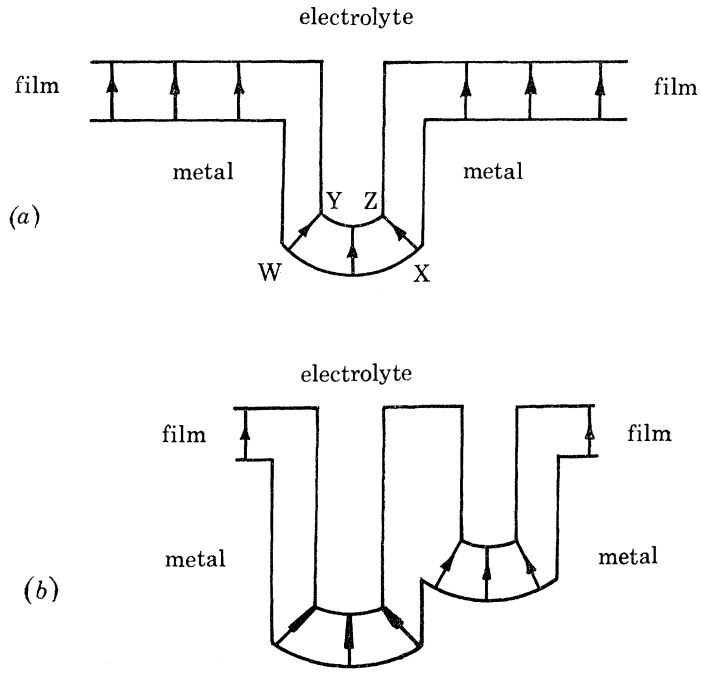

FIGURE 20. Schematic representation of the anodic film during initiation of the major pores: (a) single pore initiated, and (b) development of the pore and cell distributions for adjacent cells at different stages of development, showing the current distributions.

Figure 21 shows schematically three possible cases, in which the pore base has different radii of curvature. Initially it is assumed for simplicity that constant voltage anodizing prevails (although the argument is also applicable at constant current density), and that the barrier-layer thickness, b, and the solid angle, ω, remain constant as the pore diameter varies. It is supposed that r_2 is the equilibrium pore base radius of curvature under the set conditions.

The extent to which the field increases on passing from the cell base to the pore is measured approximately in the three cases by the ratio of the cell base area to pore base area, since the same current is passing through all of the surfaces, thus:

$$\frac{(r_1+b)^2}{r_1^2}; \quad \frac{(r_2+b)^2}{r_2^2} \quad \text{and} \quad \frac{(r_3+b)^2}{r_3^2}.$$

Clearly, as the radius of curvature increases, any enhancement of the field assisting dissolution at the pore base due to convergence of the lines of force there decreases and the field approaches the average field through the barrier layer, which is the

Downloaded from rspa.royalsocietypublishing.org on February 28, 2013

same everywhere. In essence, film formation occurs at a constant rate in all situations, being determined by the average field. It is balanced by field-assisted dissolution, whose rate is determined by the local field, determined by the radius of curvature of the pore base. A self-adjusting situation predominates, any tendency for the pore diameter to become too large or too small being checked by a consequent increase or decrease in the radius of curvature of the pore base. The constant pore and cell sizes, proportional to cell voltage, are a consequence of the equilibrium barrier-layer thickness and pore base radius of curvature established.

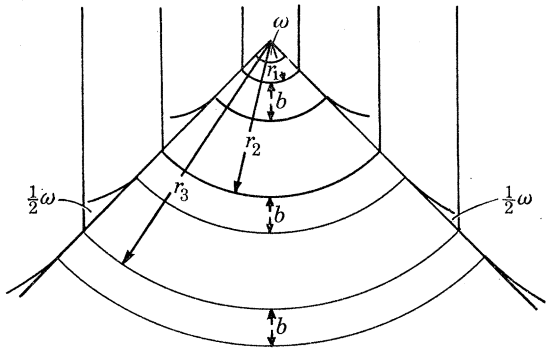

FIGURE 21. Schematic representation of three possible pore base situations, r_1, r_2 and r_3 representing the radii of curvature of the pore bases, b the constant barrier-layer thickness and ω the (constant) solid angle subtended from the centre of curvature to the pore bases. r_2 is the steady-state radius of curvature under the prevailing anodizing conditions.

In practice, slight variations in barrier-layer thickness may occur during the establishment of the steady-state pattern at constant voltage. At constant current density, relatively large changes can occur in the barrier-layer thickness, as the pores initiate, and these are reflected in the measured voltages (figure 3*a*). The initial rise is dominated by barrier-layer growth. The drop from the maximum corresponds to the initial pores having a low radius of curvature, giving a high rate of field-assisted dissolution. As the pore base radius of curvature increases with the growth of the pore diameter, the dissolution at the pore bases slows down and the rate of voltage decrease declines until the pores and barrier layer have reached their equilibrium dimensions. These changes do not invalidate the simplified argument significantly.

From the assumption that ω should be constant for all pore radii of curvature, it follows that the pore and cell bases must remain constant segments of the spheres of which they respectively form parts. That this is reasonable becomes apparent upon consideration of the field at the intersection point of two adjacent cells for the three different cases of figure 22, in which the barrier layer is of constant thickness but the proportions of the appropriate spheres occupied by the cell and pore bases vary. The unoxidized metal close to points A in figure 22 is acted upon by two components of the field, each component trying to pull the metal into different cells. In figure 22*a*, where the pore and cell bases are almost hemispheres, these two fields

Downloaded from rspa.royalsocietypublishing.org on February 28, 2013

almost cancel each other out and so there is virtually no net field acting to pull ions through the oxide towards or away from the pore base. In the absence of moving ions there is less tendency for field-assisted dissolution to propagate the pores sideways and enlarge them. As we move to figures 22*b* and *c*, however, the horizontal components of the field cancel out as before but the vertical components reinforce, causing film growth and balancing field-assisted dissolution to promote barrier layer and pore propagation into the metal. Therefore, if the segment becomes too small, the appropriate component of the field causes lateral spread of the pore, whereas if it is too large penetration into the barrier layer predominates.

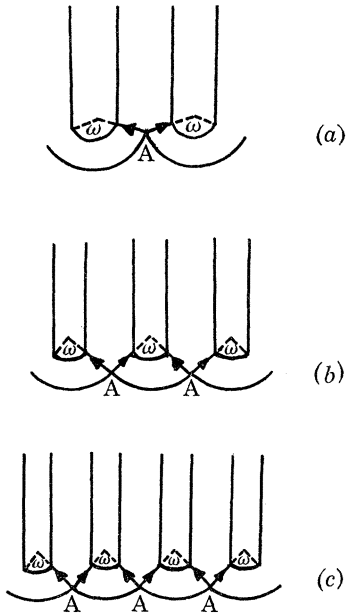

FIGURE 22. Schematic representation of three possible situations at the pore base, with the segments of the spheres occupied by the pore and cell bases of varied size (ω variable) and the barrier layer of constant thickness.

It is therefore quite clear why a constant angle θ of $\cos^{-1} 0.71$ should be obtained for the limited range of voltages under a given set of anodizing conditions, requiring a direct relationship between cell-wall thickness and barrier-layer thickness (figure 7). Until it is possible to measure field-assisted dissolution rates on plane surfaces as a function of the field, in the absence and presence of Joule heating, it does not seem possible to calculate further the interplay of film formation and film dissolution at the pore bases. An alternative approach might be to estimate the fields existing at the pore bases from their geometry (i.e. pore base area/cell base area ratio) at known anodizing voltages, and relate these to the known dissolution rates at the pore bases. The insufficient data did not warrant such calculations in the present study. The constant angle would not be expected with a larger range of fields because dissolution and formation are affected to different extents by the field.

Downloaded from rspa.royalsocietypublishing.org on February 28, 2013

(*d*) *The variation of film parameters with anodizing conditions*

The effect of increasing acid temperature and concentration upon the morphology and structure of the porous outer layer has already been discussed. There is, however, a second more fundamental effect of the increased electrolyte aggressiveness in decreasing the voltage established across the barrier layer for a given formation current density, and consequently in *decreasing* the pore and cell dimensions at the film base. Essentially, the field is attempting to grow the film to a thickness of 1.2–1.4 nm V^{-1}, as in a barrier-type electrolyte, but the barrier layer is dissolving under the field, so a dynamic equilibrium is set up between the two processes.

TABLE 3. THE VARIATION OF BARRIER LAYER nm V^{-1} RATIO WITH ACID CONCENTRATION AND TEMPERATURE AT CONSTANT CURRENT DENSITY OR CONSTANT VOLTAGE

electrolyte concentration/M	temperature/°C	nm V^{-1} at constant current density	nm V^{-1} at constant voltage
0.4	20	0.89	1.14
0.4	25	0.90	1.09
0.4	30	1.05	1.04
0.4	25	0.90	1.09
1.5	25	1.10	1.04
2.5	25	1.17	0.82

Calculation of nm V^{-1} ratios for the barrier-layer thickness, using data in figures 8 and 9, shows opposite trends for the constant current density and constant voltage cases (table 3).

Formation at constant current density implies a constant growth rate and an essentially constant field across a given oxide. Consequently, the decreasing barrier-layer thickness upon increasing the electrolyte concentration and temperature is mainly due to the increased dissolution rate under the field at the barrier-layer/electrolyte interface. The lower voltage set up requires a larger number of smaller cells and pores. Table 3, however, also shows that the nm V^{-1} ratio increases with acid aggressiveness at constant current density, implying that ionic conduction becomes easier under the set current, owing to a slightly reduced field being required. The effect, presumably due to the structural changes described earlier, involving water, anion incorporation or submicro-pore formation in the barrier layer, is not particularly large. This probably implies that most of the ionic current is transported through the microcrystallites, rather than through the intercrystallite regions which could vary considerably in properties.

At constant voltage, however, both the field (dependent on the current density established) and the rate of oxide dissolution are able to vary when changing from one set of conditions to another. So, any increase in the dissolution rate would also cause an increase in the growth rate in order to maintain the constant voltage applied to the system. This possibility of mutual readjustment explains why the

Downloaded from rspa.royalsocietypublishing.org on February 28, 2013

trends observed in the barrier layer, pore and cell dimensions (figure 8) are less severe than for constant current density (figure 9). In constant voltage anodizing increased acid aggressiveness decreases the nm V^{-1} ratio. This is mainly due to field-assisted dissolution at the pore bases increasing the current density and hence the field under the more severe conditions. The effect would, however, tend to be moderated by a relatively minor increase in the nm V^{-1} ratio due to increased ionic conductivity with enhanced film contamination, as seen at constant current density. Contamination of the anodic film could itself affect its field-assisted dissolution rate.

Hunter & Fowle (1954*b*) also found, by an indirect method, that under constant voltage operation the nm V^{-1} ratio falls from about 1.3 at 15 °C to 1.2 at 75 °C in 0.25 M chromic acid, but it does not alter with voltage at a given temperature. In sulphuric acid it falls from 1.1 in 0.5 M acid to 0.8 in 40 % acid and, in 1.5 M acid, from 1.0 at 5 °C to 0.9 at 70 °C. However, they found no effect with change of current density.

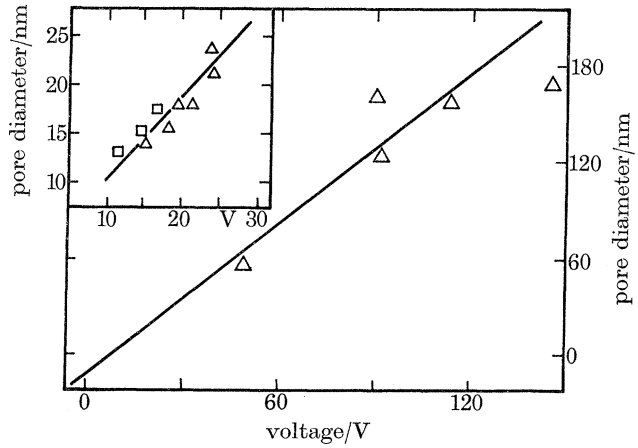

FIGURE 23. The variation of pore diameter with anodizing voltage for films formed in sulphuric acid (12 to 24 V), oxalic acid (50 V) and phosphoric acid (90 to 145 V) (low voltage values inset). △, the present results; □, results of Paolini *et al.* (1965).

Clearly the barrier-layer thickness set up during oxide growth, determined by the influence of the anodizing variables upon the steady-state voltage established, largely decides the cell and pore morphology by a simple geometrical mechanism. The detail of the composition and structure of the film material only have secondary effects to the extent to which they influence Al_2O_3 formation and dissolution rates at the pore bases under the field. The effect of using a different electrolyte type, or of changing it during a run is really an extreme case of altering the aggressiveness of the electrolyte, although doubtless minor effects of the film composition on formation and dissolution rates would be observed. This means that the pore and cell diameters should be largely independent of the acid type, and depend only on the voltage set up, as is indeed approximately confirmed in figure 23 for three acids. The corresponding

Downloaded from rspa.royalsocietypublishing.org on February 28, 2013

cell nm V^{-1} values are 2.77, 2.48 and 2.65 for phosphoric, oxalic and sulphuric acids respectively (O'Sullivan 1968).

Under the standard conditions used for each acid here (O'Sullivan 1968) and by Keller *et al.* (1953), the acid aggressiveness decreases in the order

sulphuric > oxalic > phosphoric,

as reflected in the equilibrium barrier layer nm V^{-1} ratios observed and in the equilibrium barrier-layer thicknesses established. It is therefore a natural consequence of the theory that the pore dimensions next to the barrier layer, as well as the barrier layer and cell dimensions, are larger for milder electrolytes during formation at constant current density.

(*e*) *The effect of changing the anodizing voltage during growth*

Murphy & Michelson (1962), Murphy (1967) and Michelson (1968) found that, upon lowering the voltage at some stage of steady-state anodizing, the recovery time depends upon both the initial and final voltages, as well as the difference between them, and upon the rate at which the voltage was lowered. It is further influenced by the temperature of the acid in which recovery occurred and upon the concentration of the acid in which the initial film was made, as well as upon the treatment of the film between growth and recovery. They explained these observations during sulphuric acid anodizing by proposing that protons produced by reaction between counter-migratory Al^{3+} and OH^- ions in the film act as a resistance in the barrier layer to further growth at the lower field, and only when the space charge has been dissipated can further growth occur.

In the present work, although many of the above findings are substantiated, there is direct evidence that film thinning does occur during the induction period before the current rise, contrary to their hypothesis. They measured film capacitances during the recovery time and the shape of the capacitance–time curves was similar to that of the current–time curves, little current flowing in the initial stages. However, capacitance–time curves of this shape are well known for approximately uniformly thinning oxides (Heine & Pryor 1963; Brock & Wood 1967). When plotted in terms of reciprocal capacitance (which is proportional to film thickness) versus time, they are essentially linear. Current–time curves on the other hand would only be expected to give an indication of film thinning when a relatively large current could pass, i.e. towards the end of the thinning period, when the field is sufficiently high again to maintain substantial ionic movement. Thus, although the concept of proton space charges is becoming increasingly popular (Vermilyea 1965), for example to explain rectification in barrier layers, it is not required to explain the recovery phenomenon. The data of Murphy & Michelson have very recently been independently and similarly criticized by Diggle, Downie & Goulding (1969). Furthermore, Eigen (1959) calculated that proton mobilities are only one or two orders of magnitude less in materials similar to the present barrier layers than

Downloaded from rspa.royalsocietypublishing.org on February 28, 2013

those of electrons in metals. Consequently it would be expected that excess protons would be rather readily removed by the anodizing field, even the relatively low field present at the commencement of recovery.

The barrier to oxide growth during recovery is really the barrier layer itself, which is too thick to allow a field high enough for substantial ionic movement at the lower imposed voltage. Tables 1 and 2 clearly favour field-assisted dissolution during the recovery period (possibly thermally promoted, particularly in the later stages where the current passing is higher). This phenomenon easily explains many of the findings of Murphy & Michelson but further comment is required on several points. Thus, the dependence of the recovery time upon the concentration of acid used to form the initial film is due to its influence on the structure of this film and therefore its dissolution rate under the field during recovery. That recovery could also occur in a neutral electrolyte is partly due to the ability of such electrolytes to cause slow local dissolution under a field (Brock & Wood 1967) and partly to seepage of acid from the film into the pores during recovery, lowering the pH and increasing the dissolution rate there.

After the recovery period, the porous structure rearranges and a new distribution of pores, characteristic of the new lower voltage, is established, via pore branching, each original pore producing several smaller pores, some of which cease to function after a short time. The net result is an increase in the pore and cell population. When the voltage is increased during anodizing the reverse procedure occurs. The redistribution resembles that described for the establishment of the steady-state film from the pore nucleation stages, except that here one relatively regular distribution of pores and cells is giving way to another.

When the anodizing voltage is suddenly raised the situation after the initial surge of current, which thickens the barrier layer, may be represented by the case in figure 21 where the radius is r_1. The barrier layer has thickened but the pore diameter is still that characteristic of the lower voltage. However, the increased field at the pore base, due to the increased current converging there, caused by the higher area of the cell base, enhances the pore base dissolution. The pore diameter and the pore base radius of curvature then increase until dissolution and film formation are occurring at an equal rate.

In the reverse case, when the voltage is suddenly dropped, the barrier layer must thin before substantial current can pass. However, when this has occurred, the original pore diameter is still larger than the equilibrium pore diameter. As there is no mechanism for reducing the diameter of an individual pore, new pores must initiate and take up the new equilibrium diameter. Only a very low current flows in the external circuit during the early stages of the recovery period because the field is too low for field-assisted dissolution to be much faster than the natural 'chemical' rate. As the barrier layer thins, the field increases, ions become more mobile, a current flows and dissolution becomes increasingly field-assisted. As expected, 'chemical' dissolution provides relatively uniform barrier-layer thinning but thermally enhanced, field-assisted dissolution produces or propagates pores which

Downloaded from rspa.royalsocietypublishing.org on February 28, 2013

are self-sustaining, as shown earlier. Because the field is high over the whole pore base, many pores initiate along the whole pore base and these quickly widen in diameter until certain pores are eliminated and cease to function. This is very similar to the establishment of the steady-state porous structure after the initial stages of anodizing. The number of pores initiating and then terminating is not necessarily a direct function of the voltage but depends on the electrolyte and the local field, anion content and hydrogen-bonded structure of the film, as well as any structurally or mechanically imperfect regions or irregularity in the cell and pore pattern.

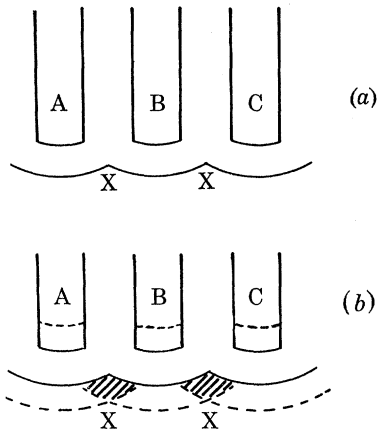

FIGURE 24. Schematic representation of (*a*) the equilibrium pore and cell dimensions and (*b*) the situation after a sudden increase in the anodizing voltage, after the barrier layer has thickened but before the pores have redistributed.

Thus, both when the anodizing voltage is suddenly lowered and when it is suddenly raised, the final result requires the elimination of certain pores. The mechanism must involve a redistribution of the current between adjacent pores, certain pores ceasing to carry current. Figure 24*a* shows schematically the equilibrium position before the voltage is suddenly raised and the dotted lines in figure 24*b* give the new extent of the barrier layer after it has thickened (ignoring the relative amounts of cation and anion movement and any initial changes in the pore base radius of curvature). If most of the metal ions in and near the shaded area near X move towards pore B, then it is propagated, whilst if they move towards pore A or C these will continue to function at the expense of B. This follows because there must be more lines of force of the field going towards the pore carrying most of the current, enhancing field-assisted dissolution, allowing propagation of the pore. Pores which eventually receive no current neither block nor propagate but become dead. The occasional branching, merging and cessation of pores seen in steady-state films presumably occurs for similar reasons but it is not entirely clear why it sometimes occurs in apparently regular porous systems.

Downloaded from rspa.royalsocietypublishing.org on February 28, 2013

5. Conclusions

(1) Pore initiation in anodic films forming at constant current density occurs by the merging of locally thickening oxide regions, which appear related to the substrate substructure, and the subsequent concentration of current into the residual thin regions.

(2) The pores grow so that their diameter remains proportional to the applied voltage as the steady state is approached.

(3) The geometrical model of Keller *et al.* (1953) is confirmed in principle but not in certain crucial details.

(4) The steady-state barrier-layer thickness, cell diameter and pore diameter are all directly proportional to the formation voltage.

(5) The barrier-layer thickness, and behaviour at the pore bases generally, are decided principally by an equilibrium set up between oxide growth in the barrier layer and field-assisted dissolution at the pore bases. The dissolution may be accelerated by local heating effects.

(6) The barrier-layer thickness and cell and pore sizes are inter-related by a simple geometrical mechanism, modified somewhat by secondary factors such as the anion content and hydrogen-bonded structure of the film.

(7) Increase or decrease of the voltage during anodizing leads to a redistribution of pore and cell populations, requiring pore merging or termination and pore initiation respectively, by mechanisms resembling (1).

(8) Relatively non-aggressive electrolytes producing porous films promote thicker barrier layers, larger cells and larger pores next to the barrier layer than aggressive electrolytes under constant current density conditions.

(9) Pore widening, film distortion and film collapse upon drying, produced by chemical dissolution during prolonged contact with the acid are more severe in aggressive electrolytes.

The authors are indebted to Professor T. K. Ross for the provision of facilities from 1965 to 1968, and for encouraging this study, and to Mr B. Vaszko for his collaboration with the electron microscopical techniques. It is regretted that Dr J. P. O'Sullivan died at a tragically early age, soon after the completion of this work. The paper is based on part of his Ph.D. thesis.

References

Amsel, G., Cherki, C., Feuillade, G. & Nadai, J. P. 1969 *J. Phys. Chem. Solids* **30**, 2117.
Applewhite, F. R., Leach, J. S. Ll. & Neufeld, P. 1969 *Corros. Sci.* **9**, 305.
Bernal, J. D. 1959 *Symposium on hydrogen bonding*, p. 7. New York: Pergamon Press.
Booker, C. J. L., Wood, J. L. & Walsh, A. 1957 *Br. J. appl. Phys.* **8**, 347.
Brock, A. J. & Wood, G. C. 1967 *Electrochim. Acta* **12**, 395.
Csokan, P. 1964 *Trans. Inst. Metal Finishing* **41**, 51.
Davies, J. A., Domeij, B., Pringle, J. P. S. & Brown, F. 1965 *J. electrochem. Soc.* **112**, 675.
Diggle, J. W., Downie, T. C. & Goulding, C. W. 1969 *J. electrochem. Soc.* **116**, 737.

Downloaded from rspa.royalsocietypublishing.org on February 28, 2013

Dignam, M. J. 1965 *J. electrochem. Soc.* **112**, 722.
Dorsey, G. A. 1968 *J. electrochem. Soc.* **115**, 1053.
Dorsey, G. A. 1969 *J. electrochem. Soc.* **116**, 466.
Eigen, M. 1959 *Symposium on hydrogen bonding*, p. 429. New York: Pergamon Press.
Franklin, R. W. 1957 *Nature, Lond.* **180**, 1470.
Franklin, R. W. & Stirland, D. J. 1963 *J. electrochem. Soc.* **110**, 262.
Ginsberg, H. & Wefers, K. 1963 *Metall.* **17**, 202.
Heine, M. A. & Pryor, M. J. 1963 *J. electrochem. Soc.* **110**, 1205.
Hoar, T. P., Mears, D. C. & Rothwell, G. P. 1965 *Corros. Sci.* **5**, 279.
Hoar, T. P. & Mott, N. F. 1959 *J. phys. Chem. Solids* **9**, 97.
Hoar, T. P. & Yahalom, J. 1963 *J. electrochem. Soc.* **110**, 614.
Hunter, M. S. & Fowle, P. E. 1954*a* *J. electrochem. Soc.* **101**, 481.
Hunter, M. S. & Fowle, P. E. 1954*b* *J. electrochem. Soc.* **101**, 515.
Keller, F., Hunter, M. S. & Robinson, D. L. 1953 *J. electrochem. Soc.* **100**, 411.
Leach, J. S. Ll. & Neufeld, P. 1969 *Corros. Sci.* **9**, 413.
Michelson, C. E. 1968 *J. electrochem. Soc.* **115**, 213.
Murphy, J. F. & Michelson, C. E. 1962 *Proceedings of Conference on Anodizing Aluminium*, p. 83. London: Aluminium Development Association.
Murphy, J. F. 1967 *Proceedings of Conference on Anodizing Aluminium*, p. 3. London: Aluminium Development Association.
O'Sullivan, J. P. 1968 Ph.D. Thesis, University of Manchester.
O'Sullivan, J. P., Hockey, J. A. & Wood, G. C. 1969 *Trans. Faraday Soc.* **65**, 535.
Paolini, G., Masoeri, M., Sacchi, F. & Paganelli, G. 1965 *J. electrochem. Soc.* **112**, 32.
Renshaw, T. A. 1961 *J. electrochem. Soc.* **108**, 185.
Rogers, G. T., Draper, P. H. G. & Wood, S. S. 1968 *Electrochim. Acta* **13**, 251.
Spooner, R. C. & Seraphim, P. 1954 *Trans. Inst. Metal Finishing* **31**, 29.
Syrkin, Y. H. & Dyatkina, M. E. 1950 *The structure of molecules and the chemical bond*, p. 331. London: Butterworths.
Vermilyea, D. A. 1963 *J. electrochem. Soc.* **110**, 345.
Vermilyea, D. A. 1965 *J. phys. Chem. Solids* **26**, 133.
Vijh, A. K. 1969 *J. electrochem. Soc.* **116**, 353.
Wells, A. F. 1952 *Structural inorganic chemistry*, 2nd ed. p. 37. Oxford: Clarendon Press.
Wood, G. C., O'Sullivan, J. P. & Vaszko, B. 1968 *J. electrochem. Soc.* **115**, 618.
Wood, G. C. & O'Sullivan, J. P. 1969 *J. electrochem. Soc.* **116**, 1351.
Wood, G. C. & Pearson, C. 1967 *Corros. Sci.* **7**, 119.
Zalivalov, F. P., Tyukina, M. N. & Tomashov, N. D. 1961 *J. Russ. Phys. Chem. Soc.* **35**, 429.

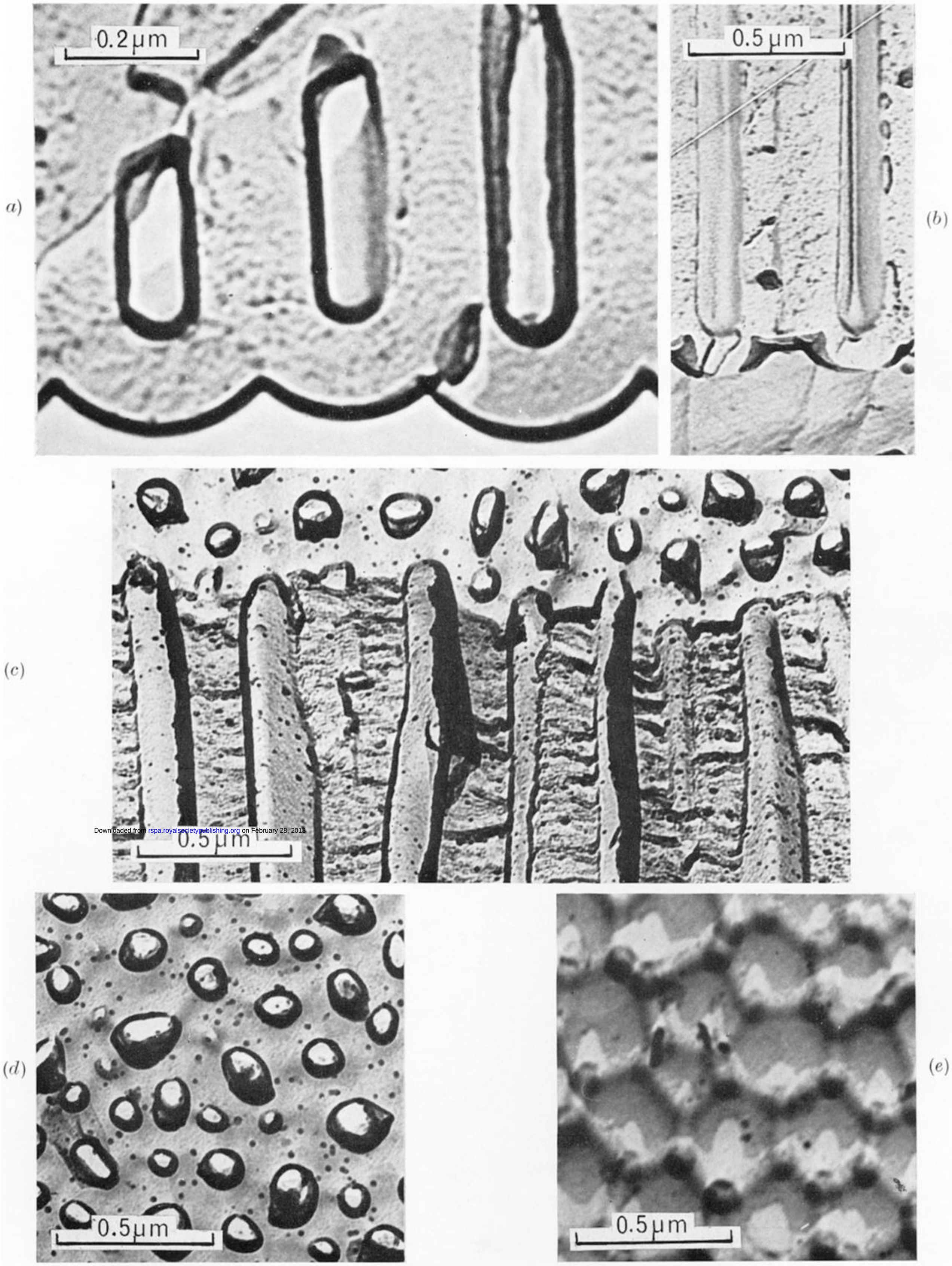

Downloaded from rspa.royalsocietypublishing.org on February 28, 2013

FIGURE 1. Replica electron micrographs of anodic films formed in phosphoric acid, showing general film characteristics: (*a*) section near barrier layer; (*b*) section with metal attached to the film base; (*c*) section near outer surface; (*d*) film outer surface; (*e*) metal surface after removal of the film. The films were formed at 120 V for (*a*) and (*b*), 145 V for (*c*) and (*d*) and 100 V for (*e*).

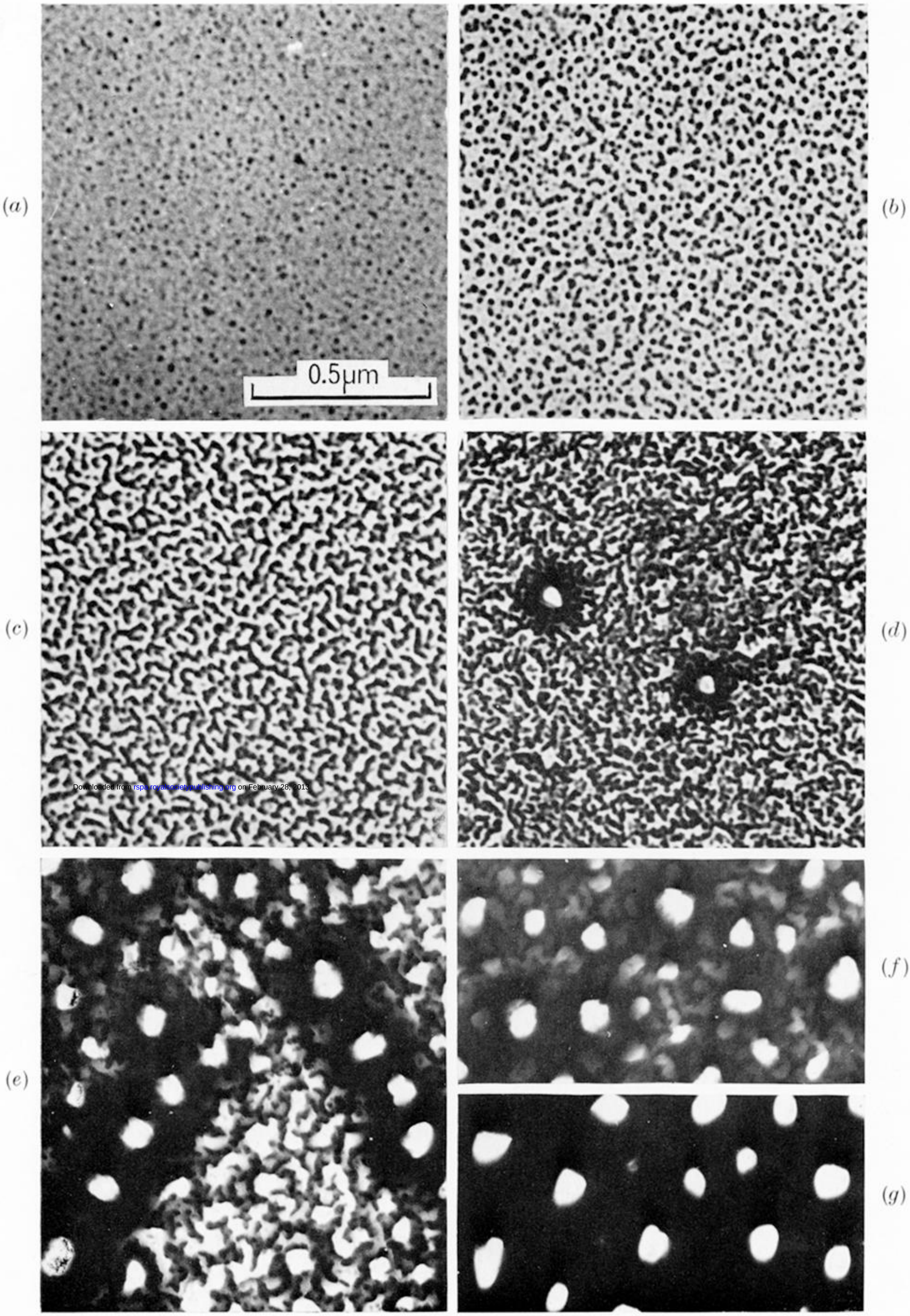

Downloaded from rspa.royalsocietypublishing.org on February 28, 2013

FIGURE 5. Transmission electron micrographs of films grown at 50 A m^{-2} in 0.4 M phosphoric acid at 25 °C for (*a*) 40 s, (*b*) 80 s, (*c*) 120 s, (*d*) 160 s, (*e*) 200 s, (*f*) 280 s and (*g*) 330 s, showing 'nuclei', incipient pores and major pore development.

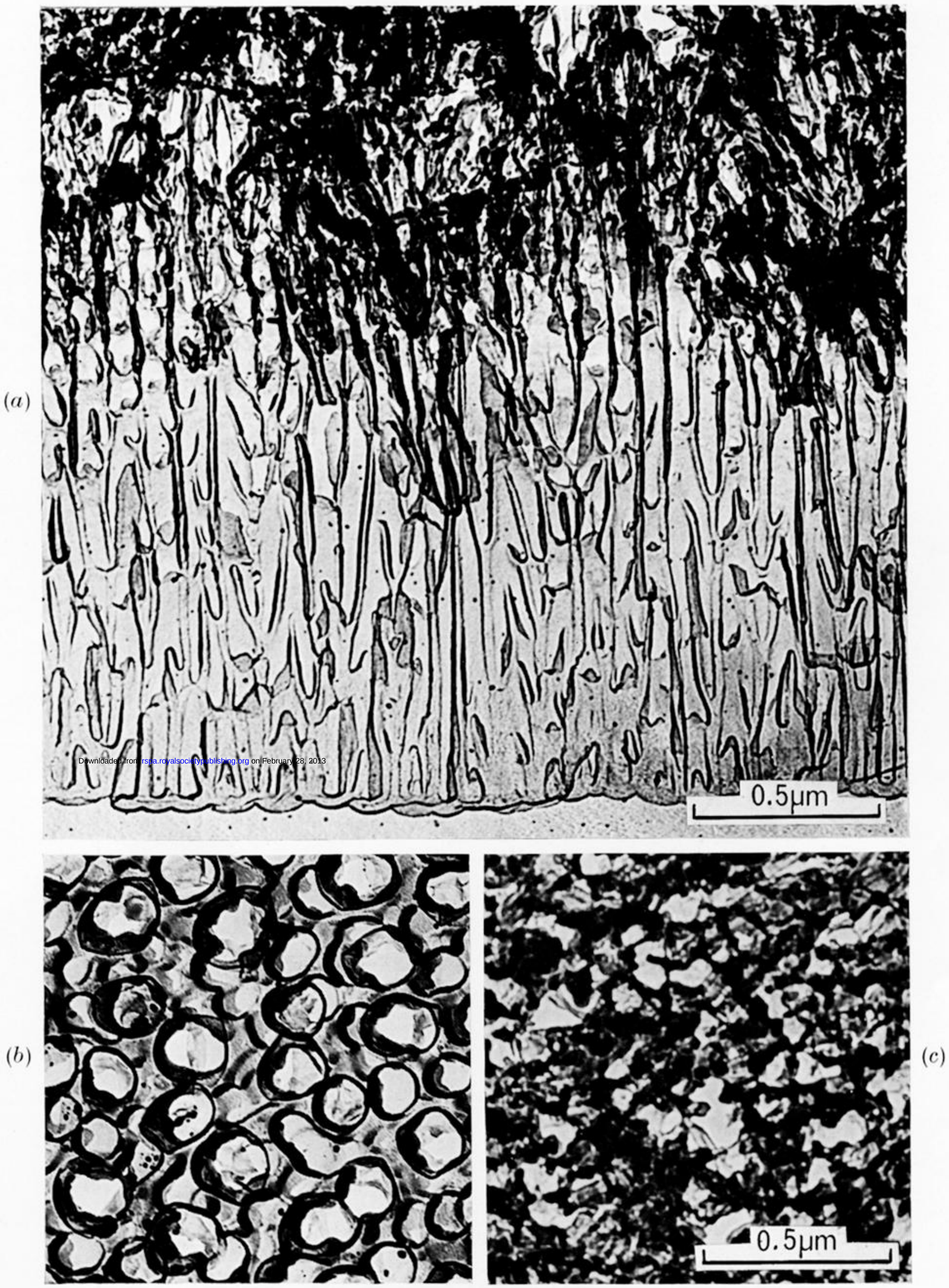

Downloaded from rspa.royalsocietypublishing.org on February 28, 2013

FIGURE 10. Electron micrographs, showing attack of outer regions of films by aggressive electrolytes: (*a*) section of 30 V film formed in 2.5 M phosphoric acid at 25 °C; (*b*) surface of film formed at 100 A m^{-2} in 0.4 M phosphoric acid at 30 °C; and (*c*) surface of film formed at 100 A m^{-2} in 2.5 M phosphoric acid at 25 °C.

(a)

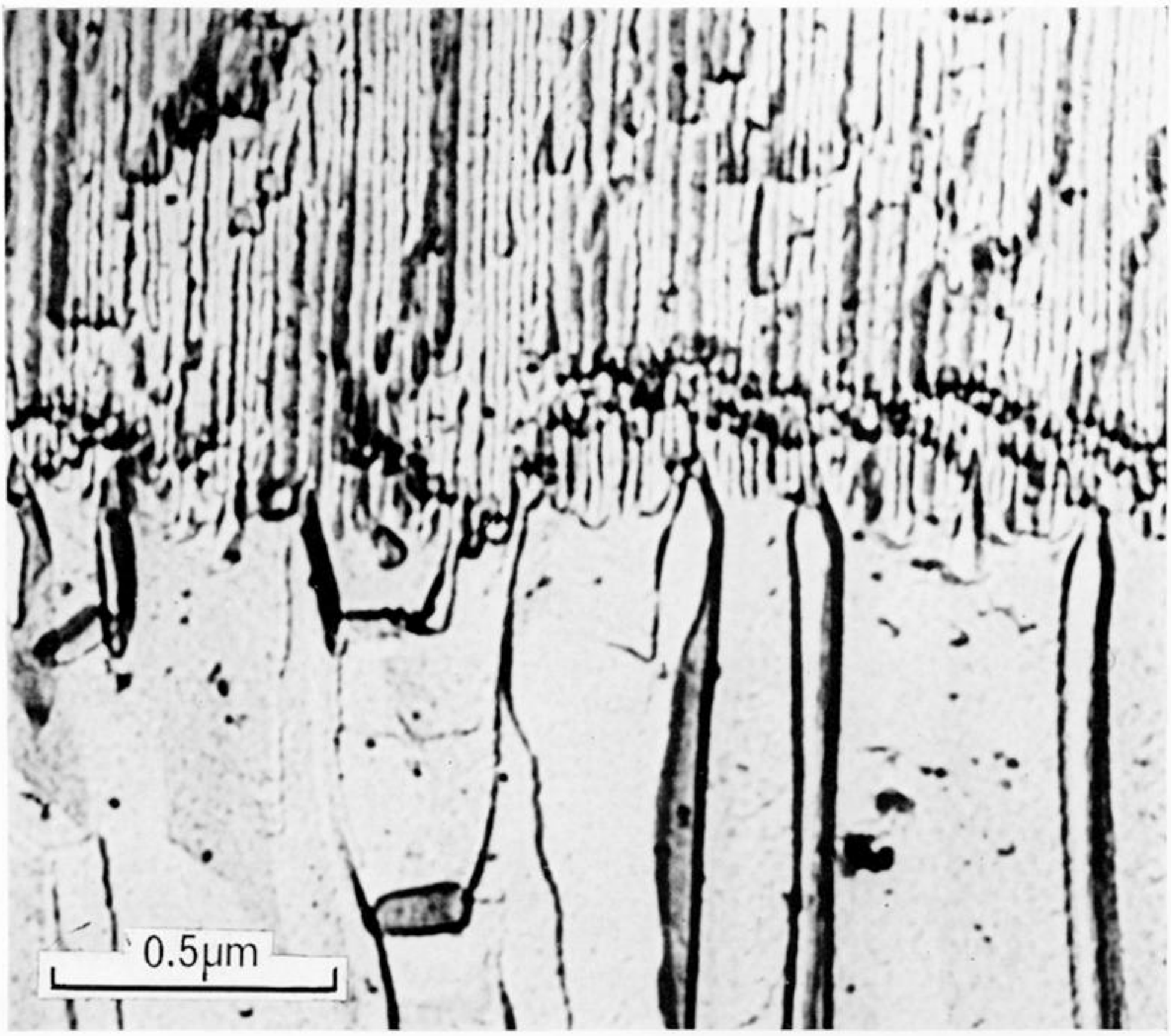

Downloaded from rspa.royalsocietypublishing.org on February 28, 2013

(b)

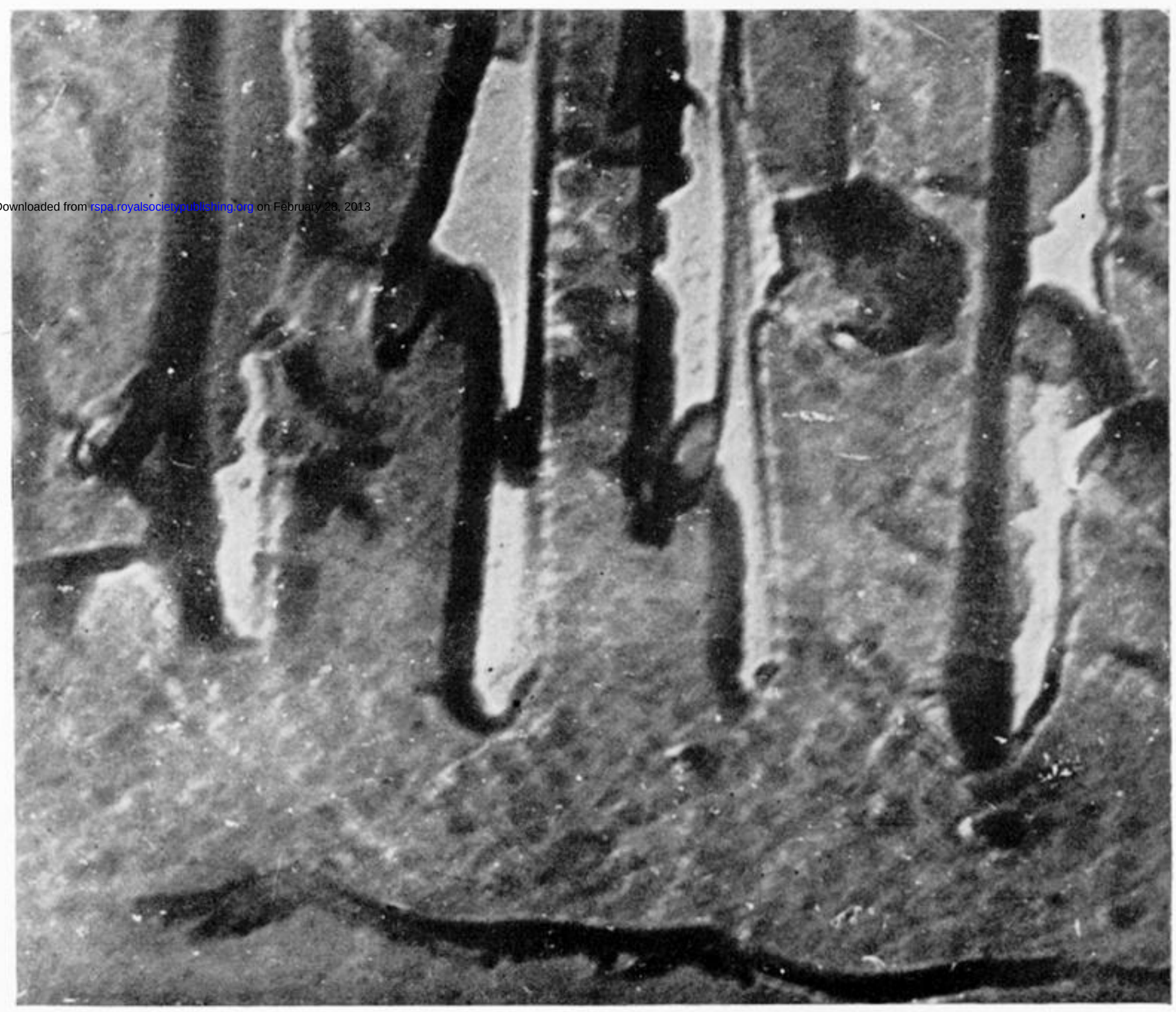

FIGURE 11. Electron micrographs of sections of 'duplex films'. (*a*) Initial formation at 18 V in 1.5 M sulphuric acid at 20 °C; reanodized at 100 V in 0.4 M phosphoric acid at 20 °C. (*b*) Initial formation at 100 V in 0.4 M phosphoric acid at 20 °C; reanodized at 260 V in 0.17 M ammonium tartrate solution (pH 7.0) at 20 °C.

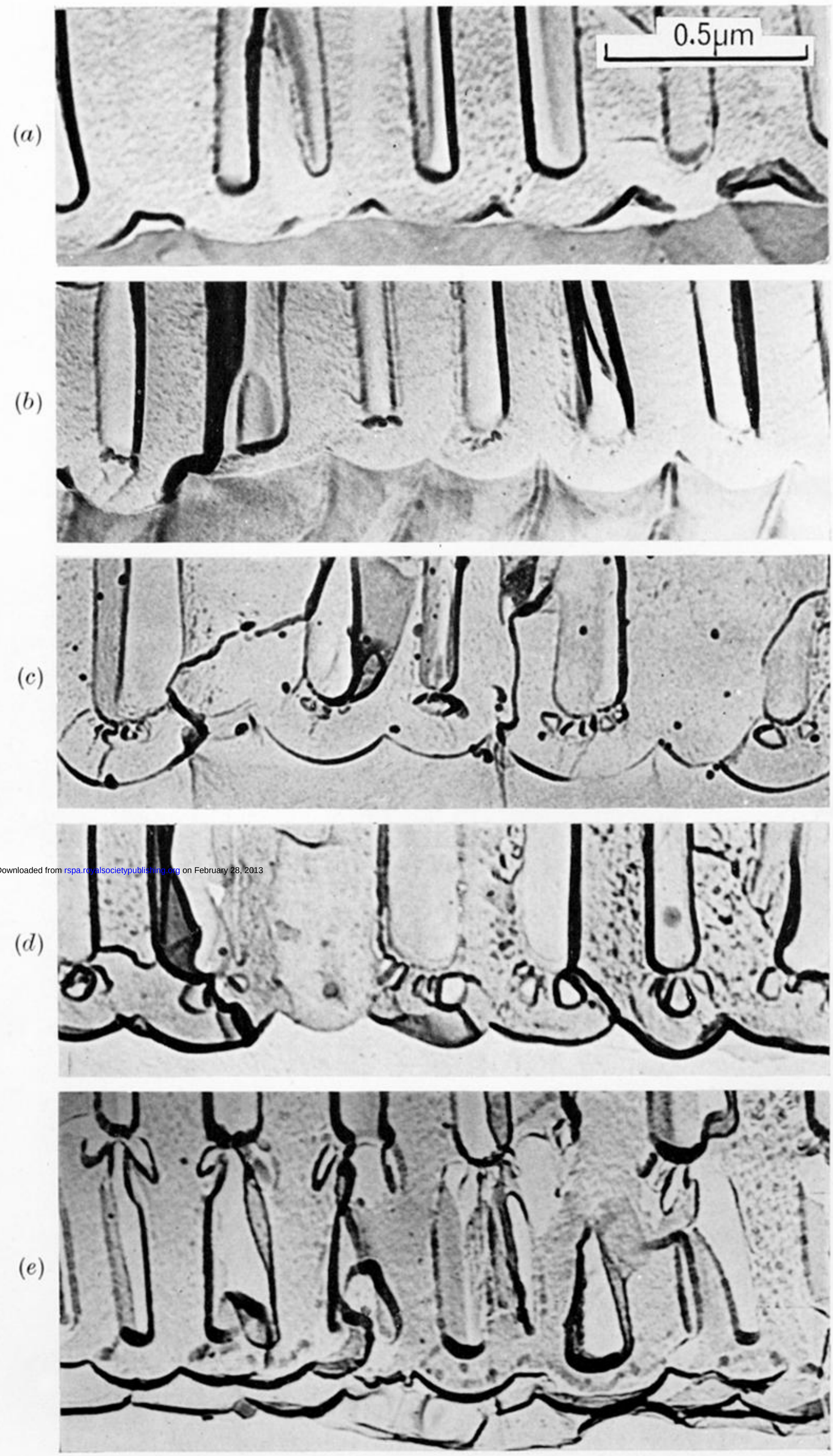

Downloaded from rspa.royalsocietypublishing.org on February 28, 2013

FIGURE 13. Electron micrographs of the sections of films at various times after a sudden voltage drop from 115 to 85 V in 0.4 M phosphoric acid at 25 °C: (*a*) 1 min, (*b*) 5 min, (*c*) 7 min, (*d*) 9 min and (*e*) 13 min after the change.

Downloaded from rspa.royalsocietypublishing.org on February 28, 2013

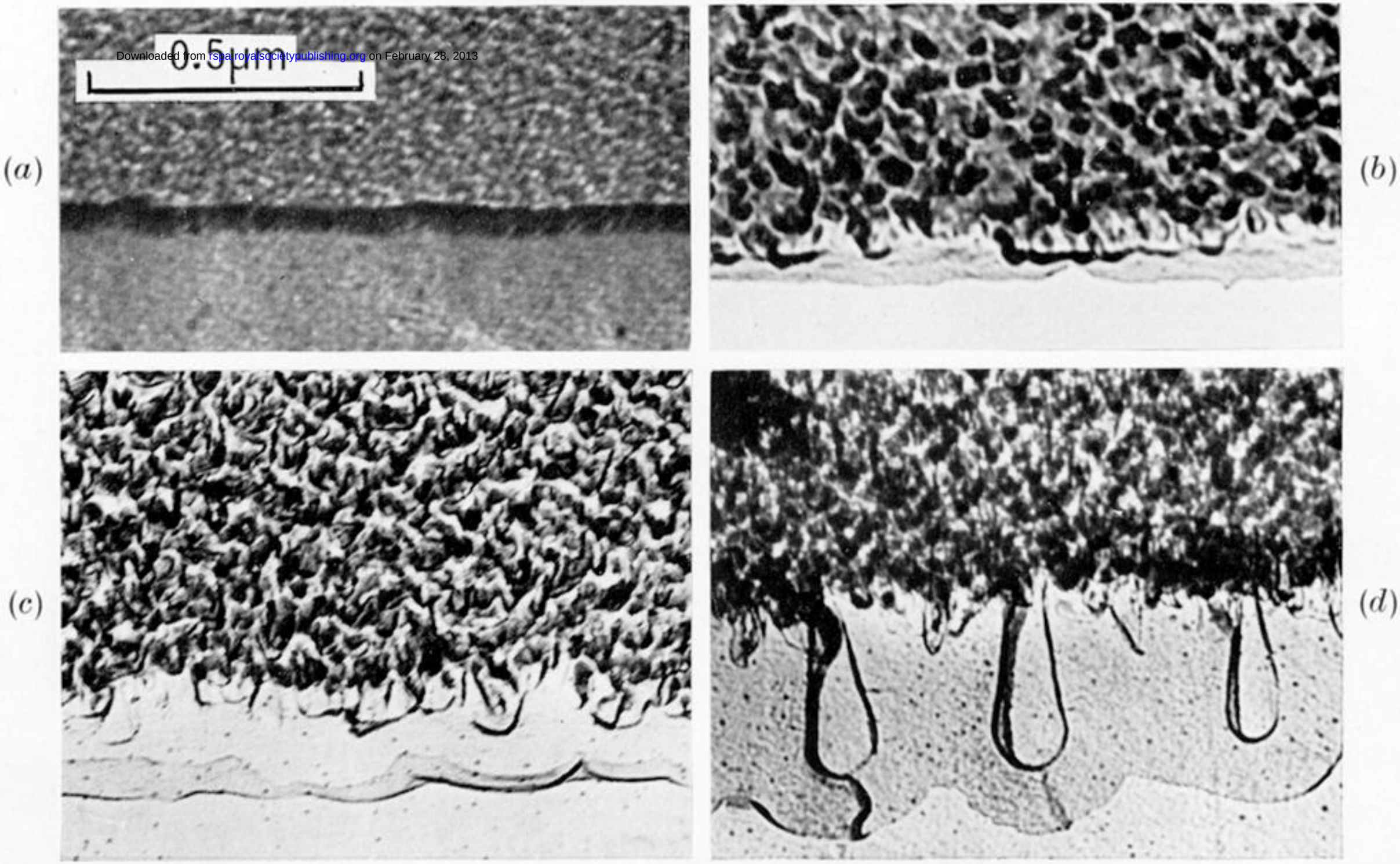

FIGURE 4. Replica electron micrographs of surfaces and sections of films grown at 50 A m^{-2} in 0·4 M phosphoric acid at 25 °C for (*a*) 40 s, (*b*) 80 s, (*c*) 200 s, and (*d*) 280 s, showing pore initiation and widening of pore diameter with increasing voltage.

Downloaded from rspa.royalsocietypublishing.org on February 2013

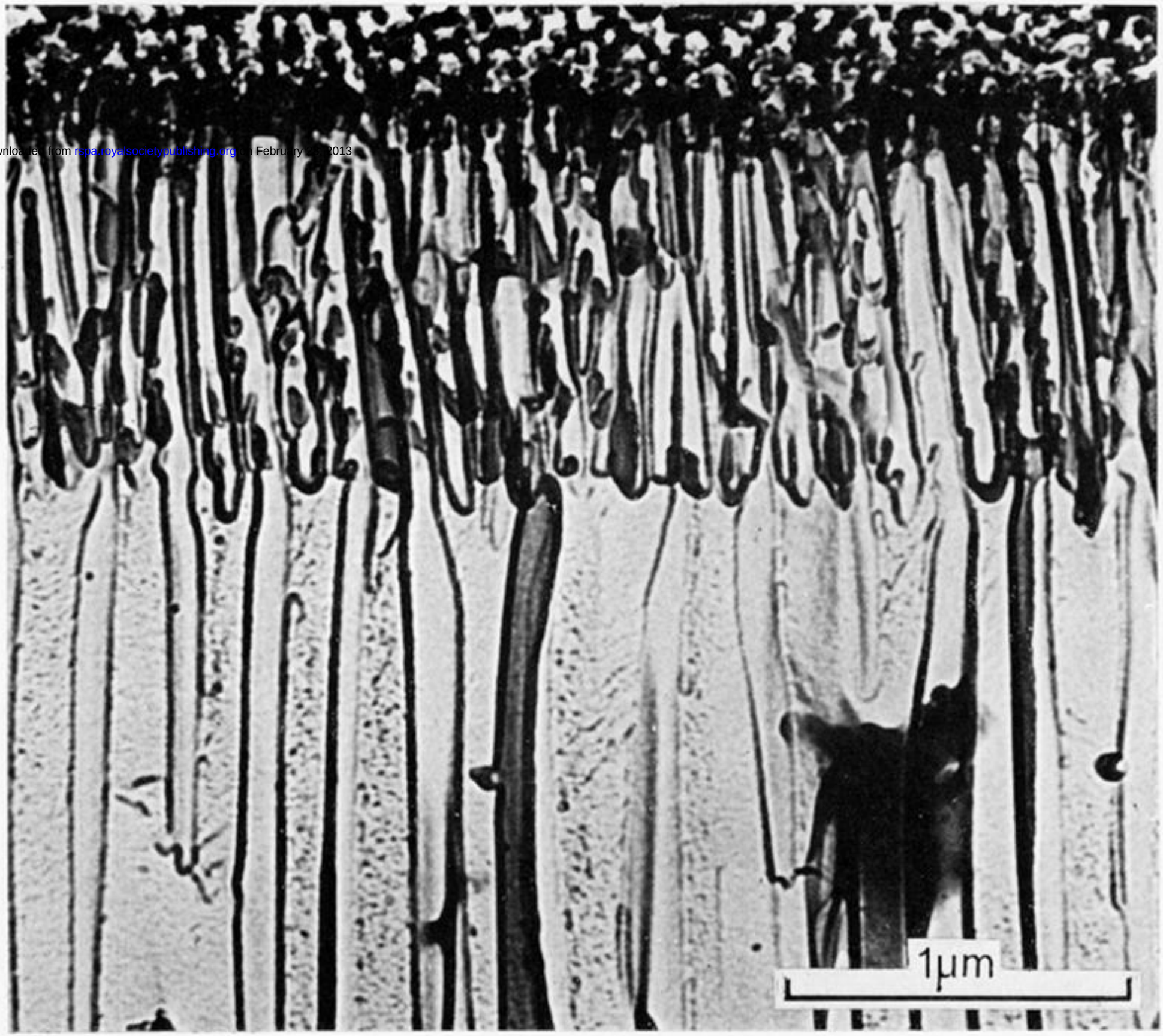

FIGURE 15. Electron micrograph of the section of a film grown in 0.4 M phosphoric acid at 25 °C for 30 min at 85 V, followed by 20 min at 115 V.